OAK RIDGE NATIONAL LABORATORY

MANAGED BY UT-BATTELLE FOR THE DEPARTMENT OF ENERGY

Gary L. Bell, Ph.D.
Fusion Energy Division
P.O. Box 2008, Bldg. 4508, Rm. 271
Oak Ridge, TN 37831-6092
(865) 241-4400
E-Mail: bellgl@ornl.gov

August 30, 2004

AGR-1012

Dr. Madeline A. Feltus
Manager, Advanced Gas Reactor
NE-20, Building GTN
Department of Energy
1000 Independence Avenue, SW
Washington, DC 20585-1290

Dear Dr. Feltus:

DE-AC05-00OR22725, Transmittal of Central File – ORNL/CF-04/07, "Results from ORNL Characterization of Nominal 350 μm NUCO Kernels from the BWXT 69300 Composite"

Attached is the central file ORNL/CF-04/07. This file documents the results of the ORNL activity to characterize 350 μm diameter natural uranium UCO kernels fabricated for the AGR program by BWXT, Lynchburg under contract with INEEL. This letter documents completion of Deliverable #7, "Issue a summary data report on characterization of 350 μm diameter NUCO kernels fabricated by BWXT," due 31Aug04, in the internal planning package AGR04-3.1.4, Rev. 2.

If you have any questions, please contact me at 865-241-4400 or John Hunn at 865-574-2480.

Sincerely,

Gary L. Bell, Manager
Advanced Gas Reactor Program

GLB:jzp

Attachment

cc: E. E. Bloom
S. R. Greene
S. R. Martin, Jr. (DOE-ORO)
S. L. Milora

c/att: J. D. Hunn
R. E. Korenke (INEEL)
R. A. Lowden
R. N. Morris
P. J. Pappano
D. A. Petti (INEEL)
J. J. Saurwein (GA)
D. F. Williams
S. J. Zinkle
File-RC

OAK RIDGE
NATIONAL LABORATORY
MANAGED BY UT-BATTELLE
FOR THE DEPARTMENT OF ENERGY

ORNL/CF-04/07

Results From ORNL Characterization of Nominal 350 µm NUCO Kernels from the BWXT 69300 Composite

J. D. Hunn

June 2004

UT-BATTELLE
ORNL-27 (4-00)

ORNL/CF-04/07
Revision 0

Results from ORNL Characterization of Nominal 350 μm NUCO Kernels from the BWXT 69300 composite

J.D. Hunn, Oak Ridge National Laboratory

This document is a compilation of characterization data obtained on the nominal 350 μm natural enrichment uranium oxide/uranium carbide kernels (NUCO) produced by BWXT for the Advanced Gas Reactor Fuel Development and Qualification Program. 5 kg of kernels were produced. G73B-NU-69300R was a 4.9 kg composite. G73B-NU-69301 was a 100 g composite. Size, shape, density, and microstructural analysis were performed on samples riffled from a 100 g sublot (69300R-38) riffled by BWXT from the 69300 composite.

Table of Contents

1 Summary of Results _____ *3*

2 Size and Shape Measurement: _____ *4*

2.1 First analysis of 350 NUCO _____ **4**

2.2 Second analysis of 350 NUCO, repeat measurement _____ **14**

2.3 Third analysis of 350 NUCO, repeat measurement at higher magnification _____ **18**

2.4 Fourth analysis of 350 NUCO, repeat measurement at higher magnification using tape _ **24**

3 Density Measurement _____ *26*

4 Optical and SEM Analysis of Kernel Surface _____ *28*

5 Friability of Kernels _____ *37*

6 Optical and SEM Analysis of Kernel Polished Cross-section _____ *39*

7 EDS Mapping of NUCO Kernels _____ *43*

8 Oxide and Carbide Phase Composition by X-ray Diffraction Analysis _____ *46*

1 Summary of Results

Measurements were made using optical microscopy to determine the size and shape of the kernels. Hg porosimetry was performed to measure density. The results are summarized in Table 1-1. Values in the table are for the composite and are calculated at 95% confidence from the measured values of a random sample taken from the 69300R-38 sublot.

Table 1-1: Summary of reported values versus kernel specification.

Kernel Property	Kernel Specification		Measured Values	
	Average	Critical Limit	Average	Critical Limit
Mean Diameter (μm)	350±20	<1% <300 and <1% >400	346-347	<1% <317 and <1% >377
Aspect Ratio (D_{max}/D_{min})	NA	<1% ≥1.05	NA	5.4% ≥1.05 <1% ≥1.09
Envelope Density (g/cc)	>10.5	NA	10.78±0.06	NA

The NUCO kernel composite met all the specifications in Table 1-1 except the aspect ratio specification. This failure was due in part to broken kernels and in part to very irregularly shaped (bumpy) kernels which apparently came from one batch used for the composite. This abnormally shaped batch made up about 1/4 of the composite.

The average open porosity of the kernels was fairly low (0.34±0.14%). There appeared to be some closed porosity throughout the kernels but a quantitative measure was not obtained.

A brief study of the microstructure of the kernels in the composite showed an oxide outer layer of varying thickness related to the process batch surrounding a center region of carbide and oxide zones. X-ray diffraction showed a phase distribution of around 69 - 74 wt% oxide versus 26 – 31 wt% carbide. Most of the carbide was in the form of uranium monocarbide (UC).

2 Size and Shape Measurement:

J.D. Hunn, A.K. Kercher, and J.R. Price

Several samples were riffled from a 100 g sublot of NUCO kernels (69300R-38). Size and shape were measured by shadow imaging with an optical microscope a sample of kernels in a random plane. Image analysis software was used to find the center of each kernel and identify 360 points around the perimeter. Data was extracted as both radius and diameter. The terms "radius" and "diameter" are used loosely. "Radius" means the distance from the fit center to the edge. "Diameter" means the distance from edge to edge in a line passing through the fit center. Data for each kernel was then reported in terms of the mean radius or diameter, the standard deviation in those values, the minimum and maximum radius and diameter, and the ratio of the maximum over the minimum of those values. These values for each kernel were then compiled and the average, standard deviation, minimum, and maximum for each value was calculated. In addition to reporting the compiled data for the sample, histograms of the mean kernel radius or diameter and the aspect ratios have also been provided to show how these values were distributed in the sample analyzed.

2.1 First analysis of 350 NUCO

Figure 2-1 shows the summary data for the measured radius of 5576 kernel shadowgraphs. Figure 2-2 shows the same data reported in terms of the diameter. The difference between compiling the measurements in terms of radius versus diameter is that the radius based measurements more accurately report non-symmetric shapes. The diameter measurements dilute the effect of a local deviation in radius by adding the opposite radius (+180 degrees in polar coordinates). Because the kernels were nearly spherical, there was no significant difference in the statistically calculated mean diameter from twice the mean radius. Even the standard deviations in these values scale by a factor of two. However, the max/min aspect ratio was significantly effected. This is because these values are based on maximum and minimums as opposed to means. R_{max}/R_{min} is a more sensitive way of measuring the deviation from perfectly spherical. The R_{max}/R_{min} measurement showed a higher average aspect ratio as well as a broader distribution toward higher values. One effect that is not accounted for in these figures is the effect of the measurement uncertainty on ratios of this type which are based on selecting maximum and minimum values. This leads to an offset in the reported value that will be discussed below.

	Rmax/Rmin	Mean Radius	St. Dev. In Radius	Minimum Radius	Maximum Radius
Average	1.05	173	1	169	176
Standard Deviation	0.03	7	1	7	8
Minimum	1.02	118	1	115	120
Maximum	1.42	212	15	206	236

Rmax/Rmin	*Frequency*
1	0
1.01	0
1.02	55
1.03	1504
1.04	1751
1.05	803
1.06	440
1.07	327
1.08	201
1.09	130
1.1	108
1.11	58
1.12	42
1.13	25
1.14	32
1.15	21
1.16	11
1.17	13
1.18	10
1.19	9
1.2	4
1.21	8
1.22	2
1.23	3
1.24	1
1.25	2
More	15

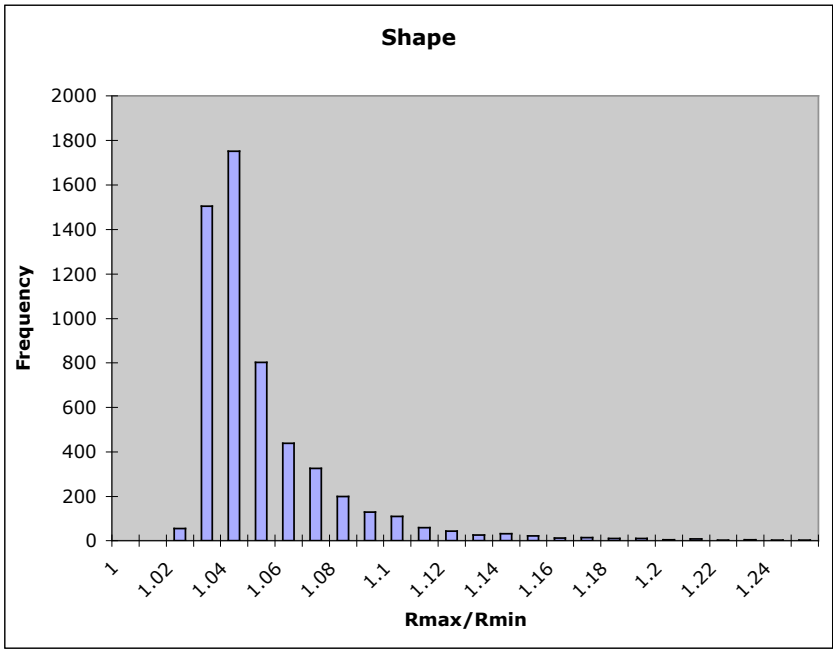

Mean Radius	*Frequency*
115	0
120	2
125	5
130	1
135	5
140	7
145	3
150	8
155	15
160	146
165	462
170	871
175	2221
180	1352
185	354
190	76
195	16
200	10
205	10
210	9
215	2
More	0

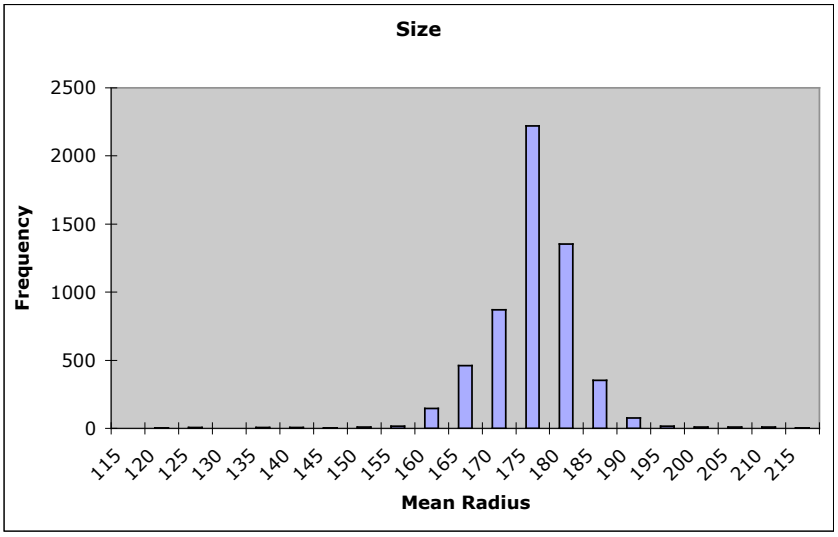

Figure 2-1: Size and shape summary for 5576 NUCO kernels. Measurements are distance from best circle fit center to edge in μm.

	Dmax/Dmin	Mean Diameter	St. Dev. In Diameter	Minimum Diameter	Maximum Diameter
Average	1.03	345	2	340	350
Standard Deviation	0.02	14	2	13	15
Minimum	1.01	235	1	232	239
Maximum	1.19	423	24	418	445

Dmax/Dmin	*Frequency*
1	0
1.01	5
1.02	1787
1.03	2200
1.04	764
1.05	355
1.06	203
1.07	83
1.08	57
1.09	39
1.1	30
1.11	14
1.12	12
1.13	10
1.14	6
1.15	2
1.16	2
1.17	1
1.18	3
1.19	1
1.2	1
More	0

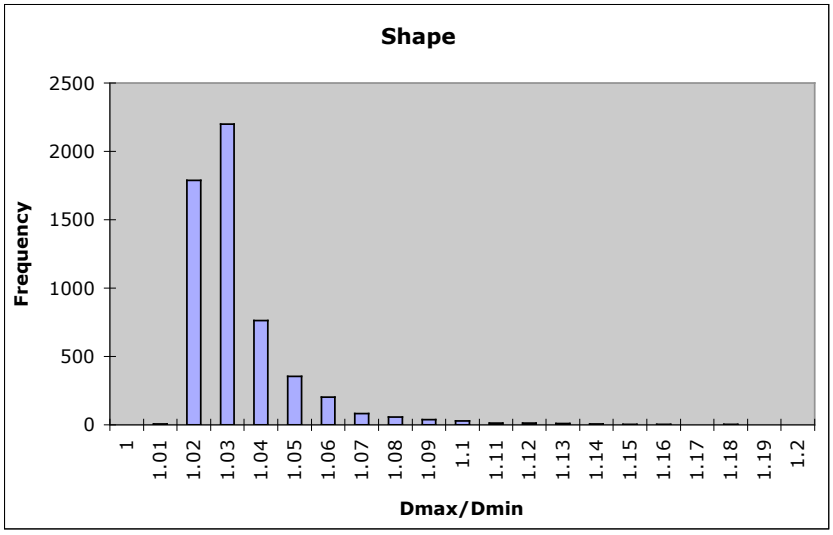

Mean Diameter	*Frequency*
230	0
240	2
250	5
260	1
270	5
280	6
290	4
300	8
310	15
320	143
330	467
340	868
350	2226
360	1347
370	358
380	74
390	15
400	10
410	10
420	9
430	2
More	0

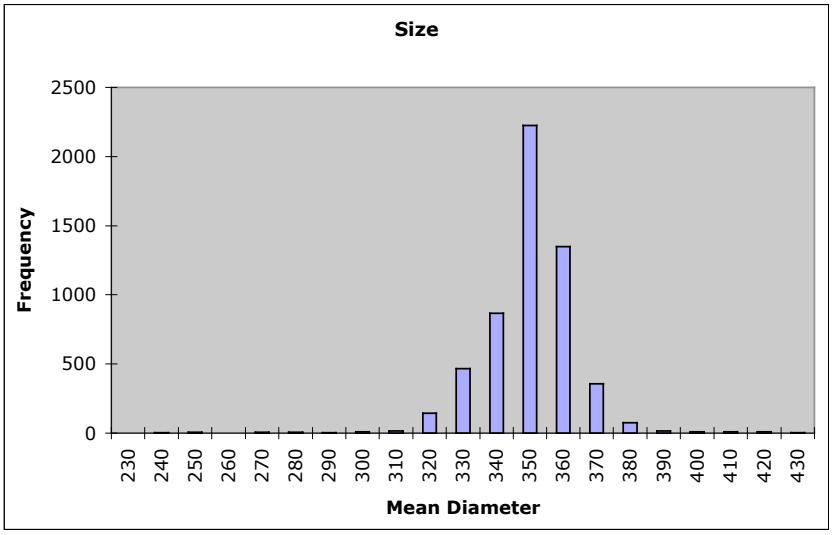

Figure 2-2: Size and shape summary for 5576 NUCO kernels. Measurements are in μm from edge to edge through best circle fit center.

As an additional way of examining the shape of the kernels, the same perimeter data measured above was also used to calculate the minimum and maximum local radius of curvature, the mean deviation from the perfect circle fit radius, and the maximum local deviation from the perfect circle fit radius. The local radius of curvature was calculated by performing a Kasa circle fit on 30° segments around the perimeter of the image. This was not a completely robust method for this calculation, but it provided a good starting point for the development of this technique. A radius of curvature that is small compared to the average radius indicates a sharp corner. A radius of curvature that is large indicates a flat. Figure 2-3 shows that most kernels had a minimum and maximum curvature slightly above or below the mean radius. The populations in the tails of the histogram indicate increasingly non-spherical particles. A possible improvement to the existing product specification might be to provide an attribute specification on the allowable percentage of kernels with a minimum radius below a certain value or a maximum radius above a certain value.

The maximum deviation in radius from the circle fit radius is another useful parameter that could be used as a fuel specification. High values would indicate unacceptable deviations in shape.

	Minimum Radius of Curvature	Maximum Radius of Curvature	Mean Deviation in Radius	Maximum Deviation in Radius
Average	111	214	1	5
Standard Deviation	29	32	1	3
Minimum	22	125	0	1
Maximum	185	489	10	47

Ave. Mean Radius = 173

Minimum Radius of Curvature	*Frequency*
20	0
30	121
40	154
50	108
60	121
70	141
80	157
90	264
100	368
110	564
120	856
130	1178
140	1055
150	438
160	44
170	3
180	2
190	1
More	0

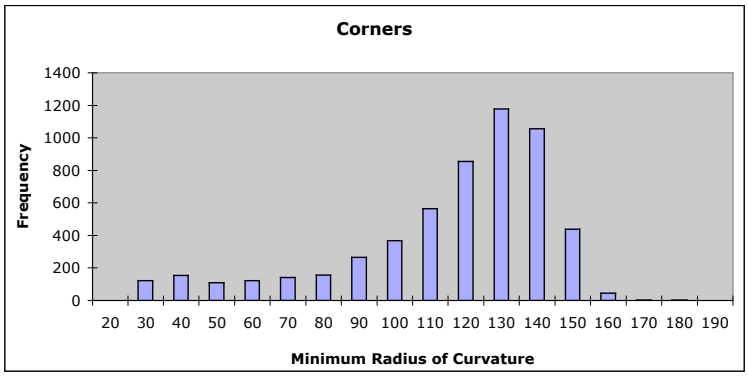

Maximum Radius of Curvature	*Frequency*
100	0
125	0
150	13
175	187
200	1998
225	1900
250	811
275	377
300	161
325	68
350	32
375	15
400	8
425	2
450	2
475	0
500	1
More	0

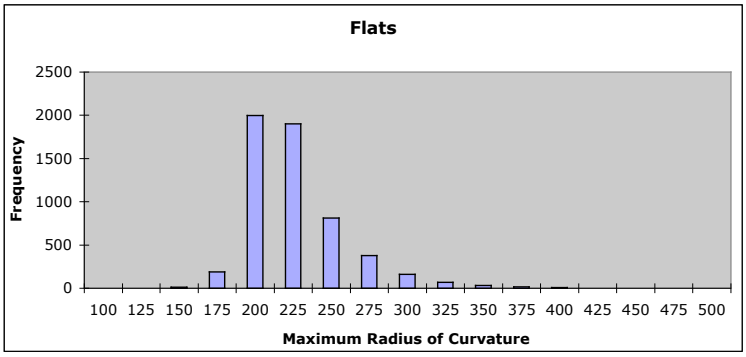

Figure 2-3: Other methods of measuring shape. Radii are in μm.

One useful feature of the data analysis in Figure 2-1 and Figure 2-2 is that it highlights the outliers in both size and shape. These images can then be easily extracted from the thousands of images used in the analysis. Figure 2-4 shows an unusually small kernel and Figure 2-5 shows an unusually large kernel imaged during the size and shape analysis. Figure 2-6 and Figure 2-7 shows several kernels that yielded high R_{max}/R_{min} values. Some of these kernels appear to have been broken during handling. Others, when viewed with a stereo microscope, appear to be badly shaped at the forming stage.

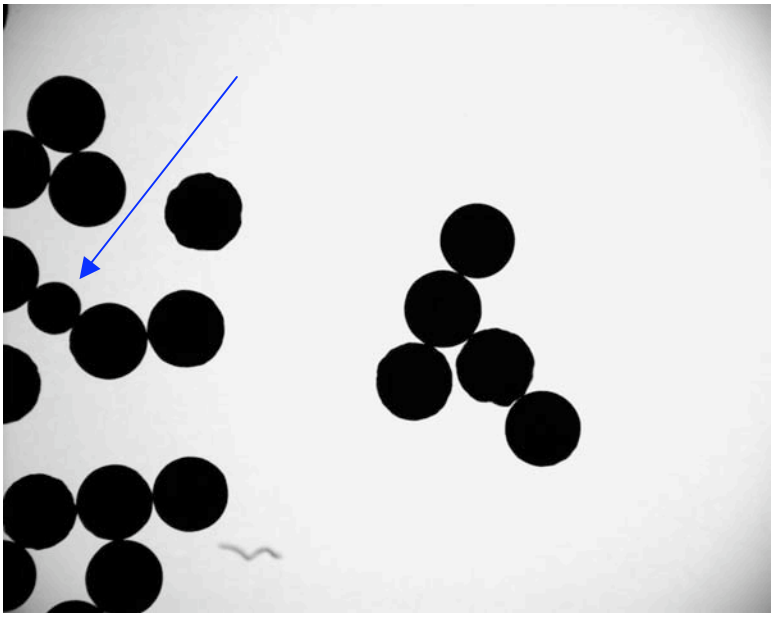

Figure 2-4: Small kernel

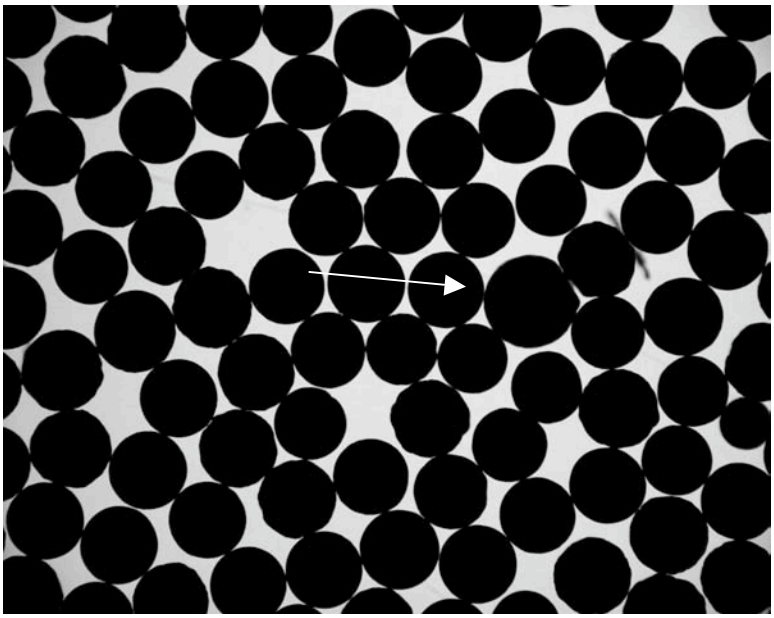

Figure 2-5: Large kernel

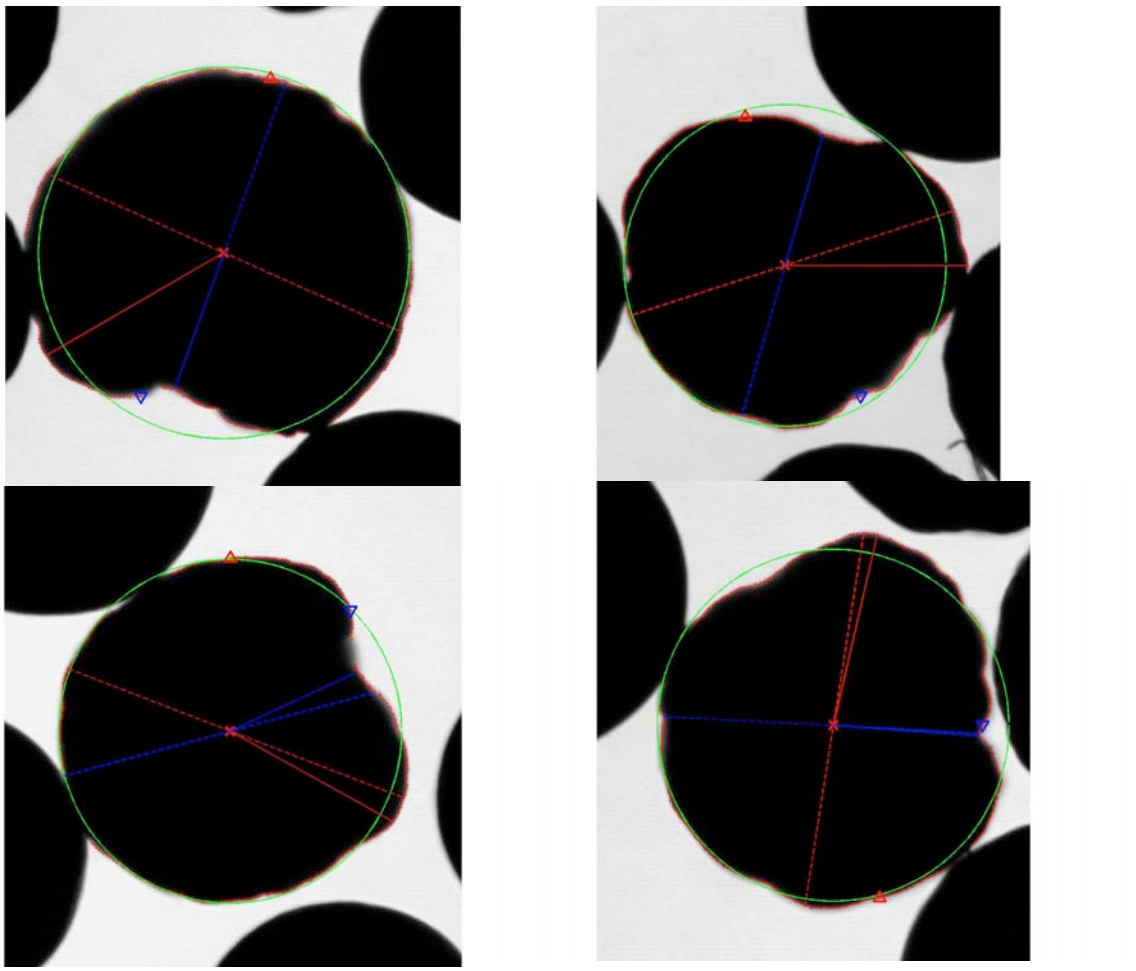

Figure 2-6: Kernels with high R_{max}/R_{min}.

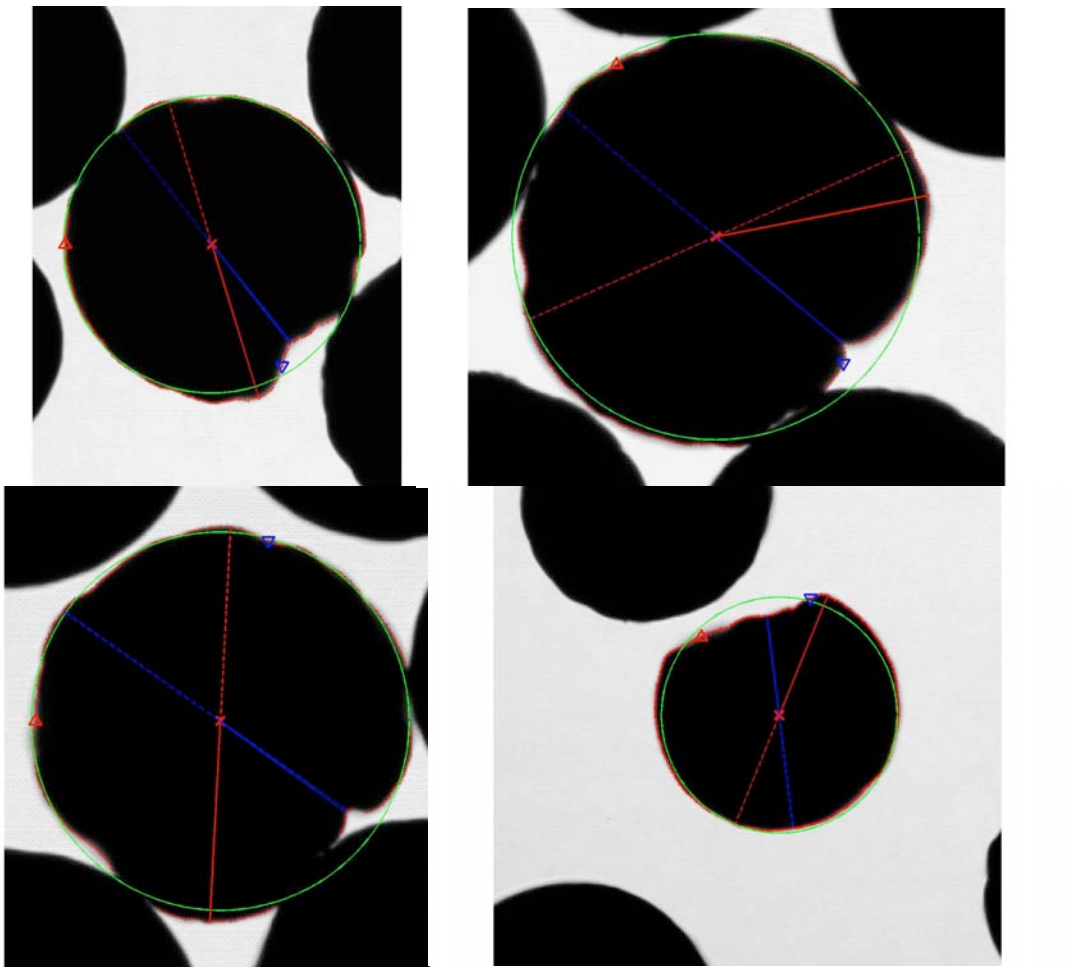

Figure 2-7: Kernels with high R_{max}/R_{min}.

A stereomicroscope was used to examine a sample of kernels to study some of the unusually shaped cases. Figure 2-8 shows a kernel where fragments have been broken off the surface. The figure also shows a number of kernels with very bumpy surfaces. These bumpy shapes appear to have occurred prior to sintering. The variations in kernel surface type will be discussed further in section 4. Figure 2-9 shows a kernel that was dimpled (probably as a gel sphere). This kernel would appear to have a "flat" in the shadowgraph imaging used for shape analysis. A kernel doublet is shown in Figure 2-10. Figure 2-11 shows a small kernel. Figure 2-12 shows an unusual case where there appeared to be an outer shell surrounding a smaller kernel "yolk". This forming anomaly may be the source of the several small ($R \approx R_{mean}/2$) kernels observed, such as that in Figure 2-11.

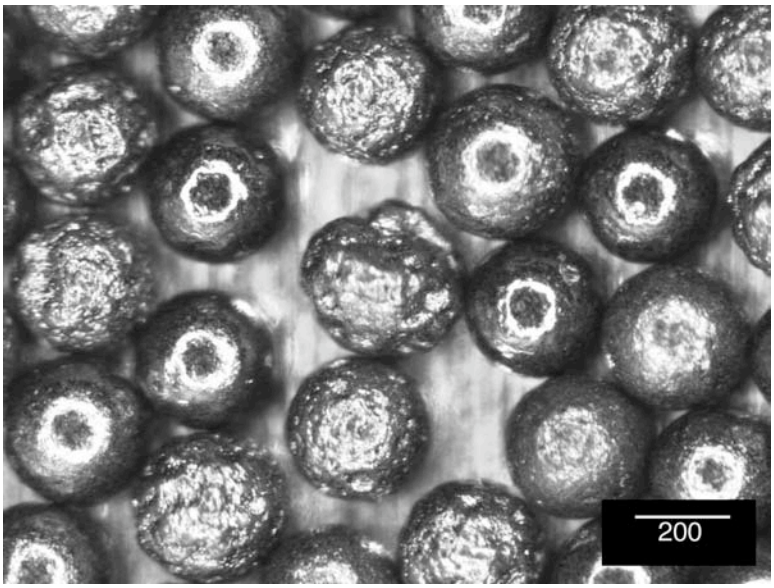

Figure 2-8: Kernel with fragments broken off (center of image).

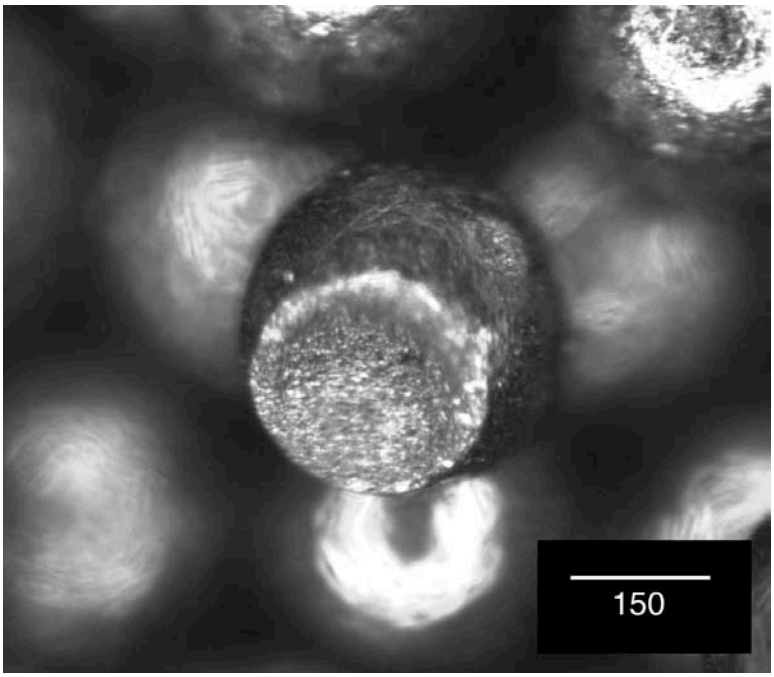

Figure 2-9: Dimpled kernel.

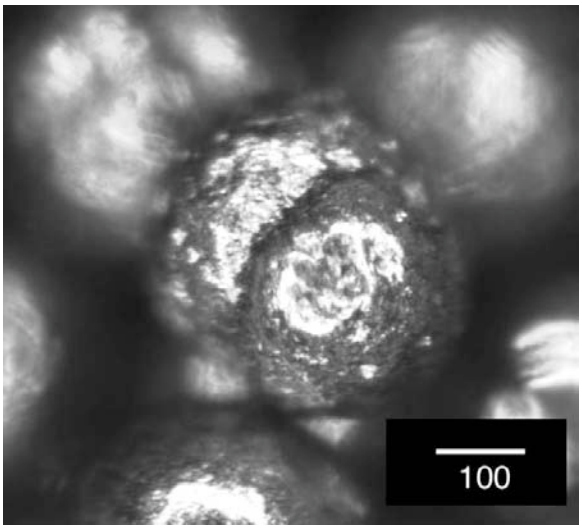

Figure 2-10: Kernel doublet.

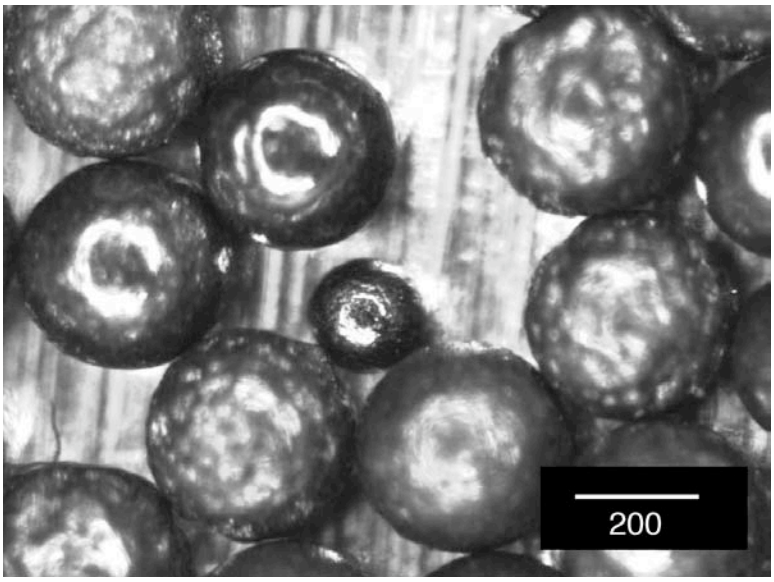

Figure 2-11: Small kernel

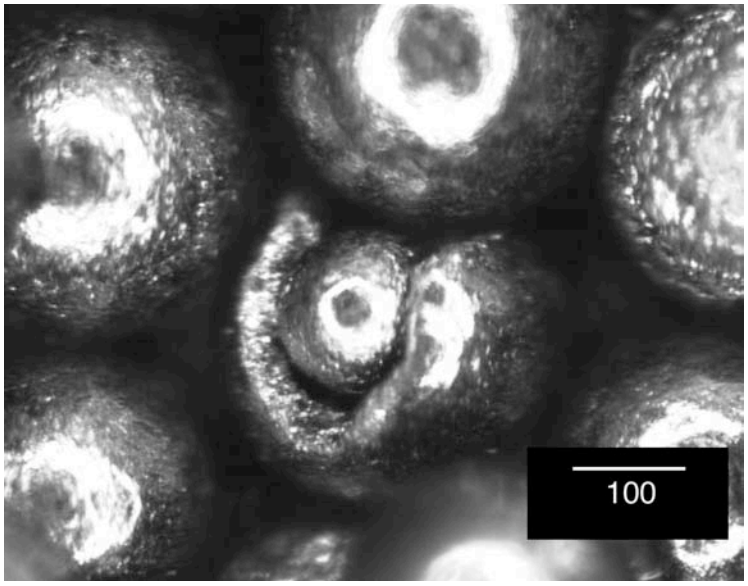

Figure 2-12: Broken shell around small kernel.

2.2 Second analysis of 350 NUCO, repeat measurement

One concern with an analysis technique that only images the kernels in one orientation is whether the analysis is sufficient to measure the size and shape of the 3-dimensional kernels. As one check for the validity of this technique, the NUCO kernels were remounted and remeasured. Figure 2-13, Figure 2-14, and Figure 2-15 show the compiled results from a second measurement on the same set of kernels measured above. The results are essentially identical in mean and standard deviation. There is some small variation in the minimum and maximum observed values, as would be expected. The reason the results show such a good match is that a large number of kernels have been observed relative to the distribution in the measured values. One way of considering the issue is that to look at 1000 kernels each in six different orientations to obtain shape and size information is statistically equivalent to looking at 6000 different kernels in only one random orientation each.

	Rmax/Rmin	Mean Radius	St. Dev. In Radius	Minimum Radius	Maximum Radius
Average	1.05	173	1	169	176
Standard Deviation	0.03	7	1	7	8
Minimum	1.02	117	1	114	120
Maximum	1.41	214	12	210	242

Rmax/Rmin	*Frequency*
1	0
1.01	0
1.02	45
1.03	1442
1.04	1767
1.05	780
1.06	457
1.07	302
1.08	219
1.09	138
1.1	107
1.11	69
1.12	38
1.13	42
1.14	25
1.15	17
1.16	19
1.17	17
1.18	12
1.19	3
1.2	6
1.21	3
1.22	3
1.23	5
1.24	3
1.25	2
More	16

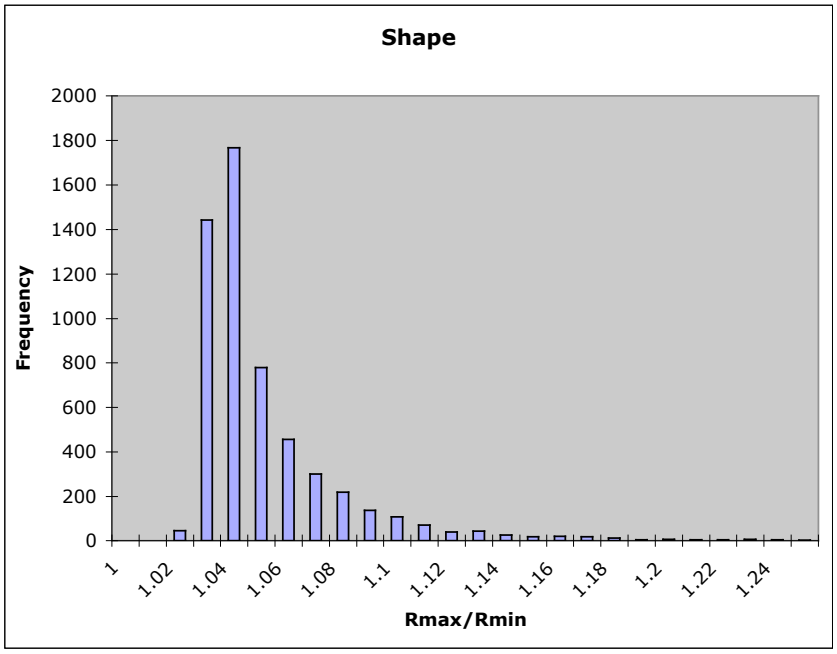

Mean Radius	*Frequency*
115	0
120	2
125	4
130	1
135	7
140	7
145	4
150	9
155	17
160	126
165	440
170	890
175	2238
180	1320
185	344
190	80
195	13
200	13
205	9
210	11
215	2
More	0

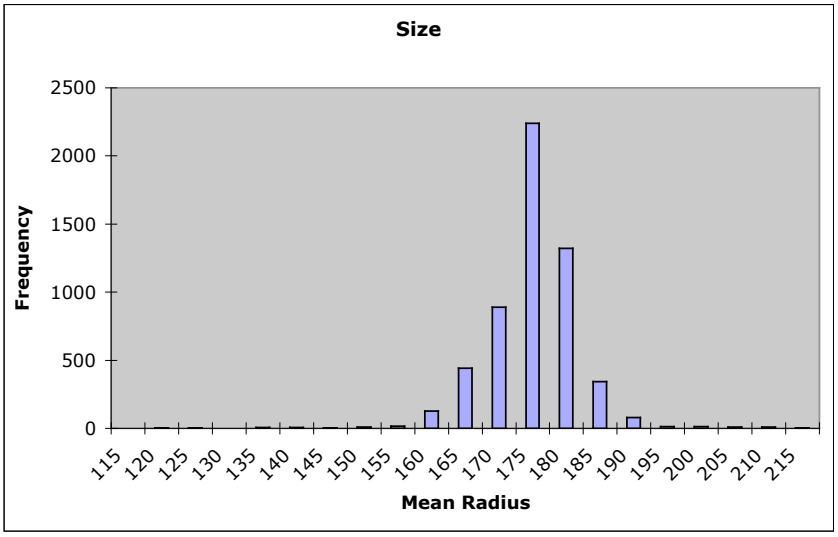

Figure 2-13: Repeat of first measurement for another random orientation. Size and shape summary for 5537 NUCO kernels. Measurements are distance from best circle fit center to edge in μm.

	Dmax/Dmin	Mean Diameter	St. Dev. In Diameter	Minimum Diameter	Maximum Diameter
Average	1.03	345	2	340	350
Standard Deviation	0.02	14	2	13	15
Minimum	1.01	235	1	231	237
Maximum	1.24	428	20	422	441

Dmax/Dmin	*Frequency*
1	0
1.01	5
1.02	1757
1.03	2167
1.04	737
1.05	382
1.06	216
1.07	112
1.08	55
1.09	37
1.1	18
1.11	11
1.12	8
1.13	8
1.14	6
1.15	7
1.16	4
1.17	3
1.18	2
1.19	0
1.2	0
More	2

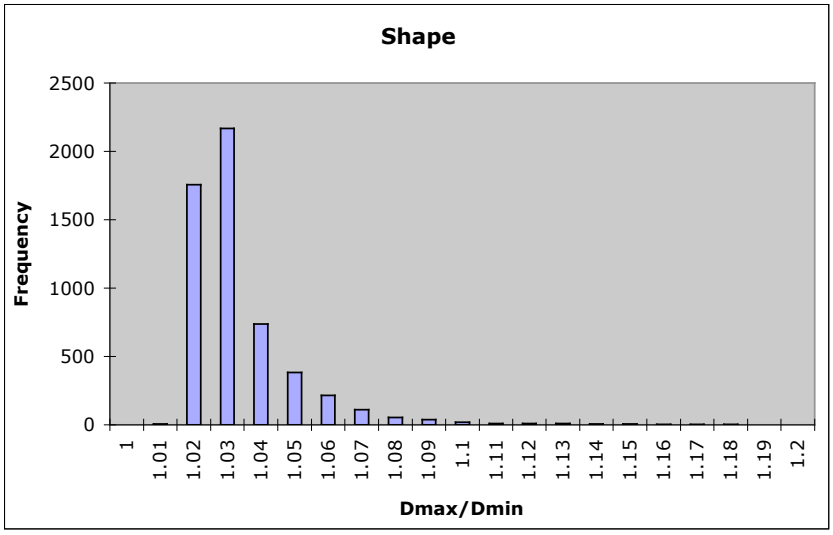

Mean Diameter	*Frequency*
230	0
240	2
250	4
260	1
270	7
280	7
290	4
300	8
310	18
320	125
330	441
340	890
350	2238
360	1317
370	348
380	78
390	15
400	12
410	9
420	11
430	2
More	0

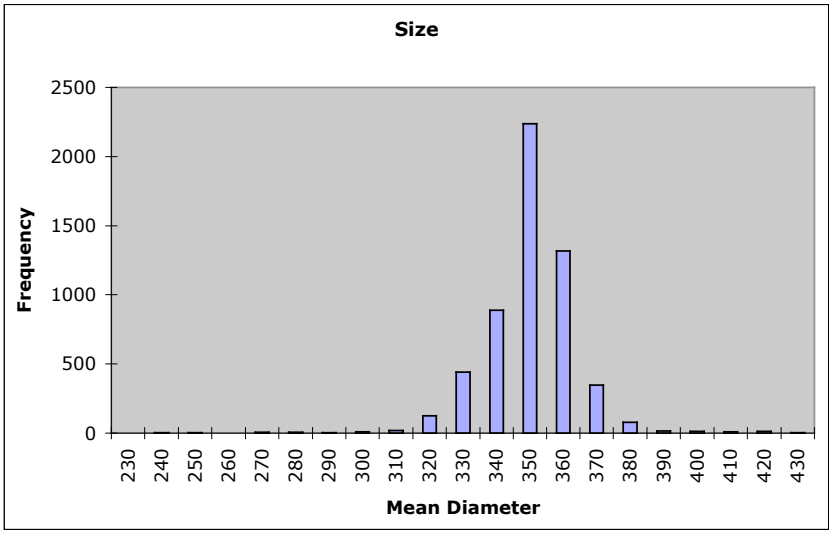

Figure 2-14: Repeat of first measurement for another random orientation. Size and shape summary for 5537 NUCO kernels. Measurements are in μm from edge to edge through best circle fit center.

	Minimum Radius of Curvature	Maximum Radius of Curvature	Mean Deviation in Radius	Maximum Deviation in Radius
Average	110	213	1	4
Standard Deviation	30	33	1	3
Minimum	22	122	0	1
Maximum	168	454	9	46

Ave. Mean Radius = 173

Minimum Radius of Curvature	*Frequency*
20	0
30	128
40	155
50	106
60	115
70	145
80	191
90	268
100	394
110	544
120	843
130	1153
140	1036
150	413
160	38
170	8
180	0
190	0
More	0

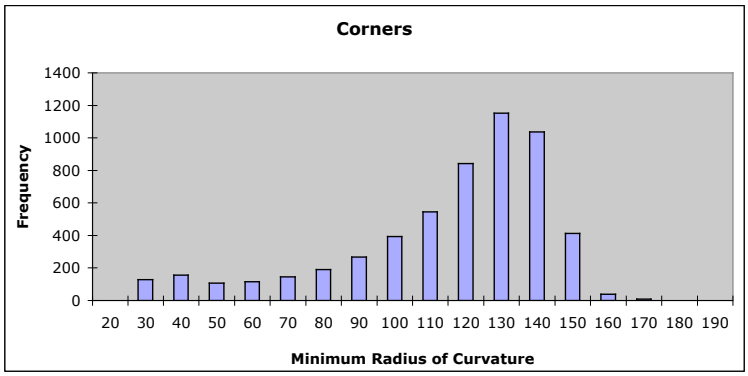

Maximum Radius of Curvature	*Frequency*
100	0
125	1
150	20
175	195
200	2037
225	1837
250	787
275	353
300	173
325	78
350	25
375	16
400	6
425	3
450	4
475	2
500	0
More	0

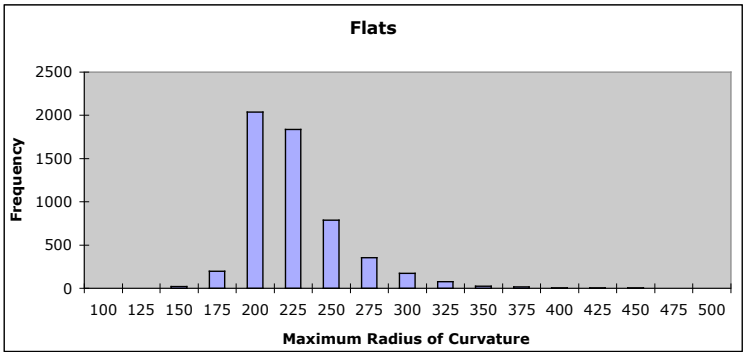

Figure 2-15: Repeat of first measurement for another random orientation. Summary of other methods of measuring the shape. Radii are in μm.

2.3 Third analysis of 350 NUCO, repeat measurement at higher magnification

As mentioned above, there is an issue with the measurement of aspect ratio that involves the uncertainty in the measurement leading to an offset in the reported value. This error stems from the non-statistical nature of using the maximum and minimum values. As in any measurement, there is an uncertainty involved in determining the position of the edge of the shadow image and thus the radius of the kernel. For the values reported above, this uncertainty was about ±1 μm. This is acceptable for the measurement of mean radius or diameter but it leads to a large systematic error when calculating the aspect ratio, as can be seen in the following calculation.

$$\frac{R_{\max}+\Delta R}{R_{\min}-\Delta R}=\frac{R_{\max}/R_{\min}+\Delta R/R_{\min}}{1-\Delta R/R_{\min}}=\left(\frac{R_{\max}}{R_{\min}}+\frac{\Delta R}{R_{\min}}\right)\left(1+\frac{\Delta R}{R_{\min}}+\left(\frac{\Delta R}{R_{\min}}\right)^2+\ldots\right)$$

$$\approx\frac{R_{\max}}{R_{\min}}+\left(\frac{R_{\max}}{R_{\min}}\right)\frac{\Delta R}{R_{\min}}+\frac{\Delta R}{R_{\min}}\approx\frac{R_{\max}}{R_{\min}}+2\frac{\Delta R}{R_{mean}}$$

ΔR is the uncertainty in the minimum and maximum radius values used to calculate the ratio. Because we are choosing the maximum and minimum values, ΔR is added to the maximum value and subtracted from the minimum value. ΔR may be several times the uncertainty in the determination of the kernel edge, which is typically ±1 pixel. For the data presented in sections 2.1 and 2.2, the offset error in the aspect ratio was $2\Delta R/R_{mean}$ = 0.01-0.02 (ΔR = 0.9-2 μm).

One way to reduce this systematic error is to reduce the measurement uncertainty by going to higher magnification. Another sample of kernels was measured at twice the magnification as used above. The results are shown in Figure 2-16, Figure 2-17, and Figure 2-18. Again, there was no significant change in the size measurement, but the shape aspect ratio shifted down as expected. The offset error in the aspect ratio for the measurement at this magnification was 0.005-0.01 (ΔR = 0.4-1 μm).

	Rmax/Rmin	Mean Radius	St. Dev. In Radius	Minimum Radius	Maximum Radius
Average	1.04	173	1	170	177
Standard Deviation	0.03	6	1	6	7
Minimum	1.01	126	0	124	128
Maximum	1.33	209	9	207	229

Rmax/Rmin	*Frequency*
1	0
1.01	0
1.02	211
1.03	1691
1.04	1137
1.05	554
1.06	369
1.07	249
1.08	142
1.09	90
1.1	73
1.11	58
1.12	35
1.13	35
1.14	18
1.15	17
1.16	9
1.17	9
1.18	2
1.19	8
1.2	0
1.21	7
1.22	4
1.23	0
1.24	0
1.25	2
More	4

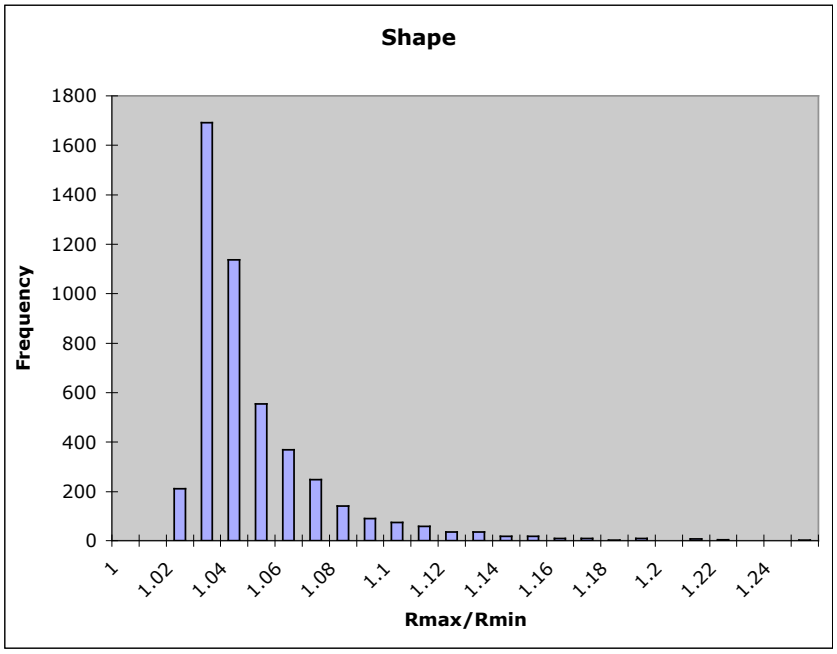

Mean Radius	*Frequency*
115	0
120	0
125	0
130	1
135	1
140	3
145	3
150	7
155	7
160	73
165	357
170	614
175	1927
180	1247
185	346
190	85
195	21
200	15
205	14
210	3
215	0
More	0

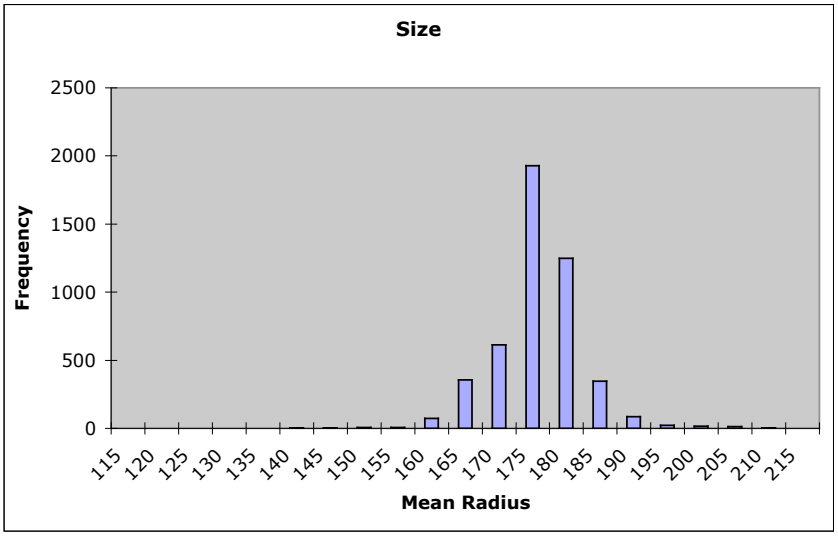

Figure 2-16: Size and shape summary for 4724 NUCO kernels measured at twice the magnification of previous measurements. Measurements are distance from best circle fit center to edge in μm.

	Dmax/Dmin	Mean Diameter	St. Dev. In Diameter	Minimum Diameter	Maximum Diameter
Average	1.03	347	2	342	351
Standard Deviation	0.02	13	1	12	14
Minimum	1.00	252	0	249	255
Maximum	1.17	419	16	416	431

Dmax/Dmin	*Frequency*
1	0
1.01	54
1.02	2082
1.03	1438
1.04	558
1.05	283
1.06	131
1.07	69
1.08	50
1.09	26
1.1	8
1.11	10
1.12	8
1.13	3
1.14	1
1.15	0
1.16	1
1.17	0
1.18	2
1.19	0
1.2	0
More	0

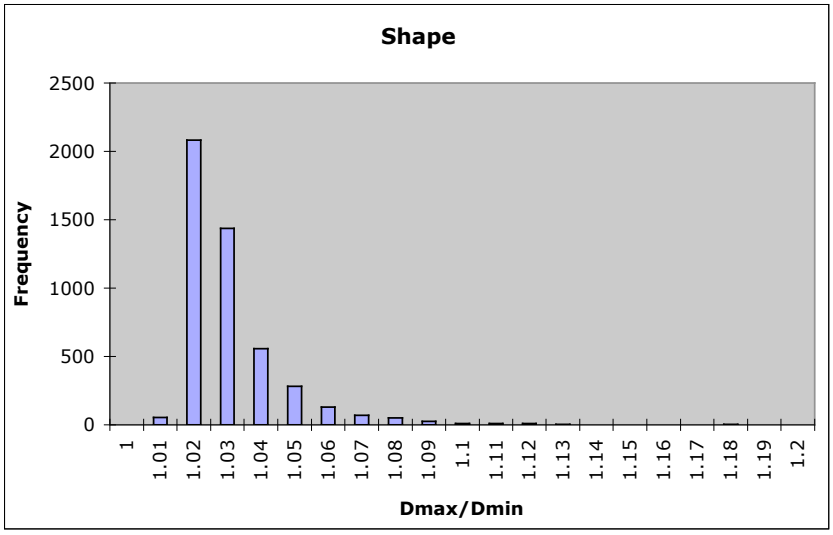

Mean Diameter	*Frequency*
230	0
240	0
250	0
260	1
270	1
280	3
290	3
300	6
310	7
320	73
330	360
340	612
350	1929
360	1251
370	337
380	88
390	21
400	15
410	14
420	3
430	0
More	0

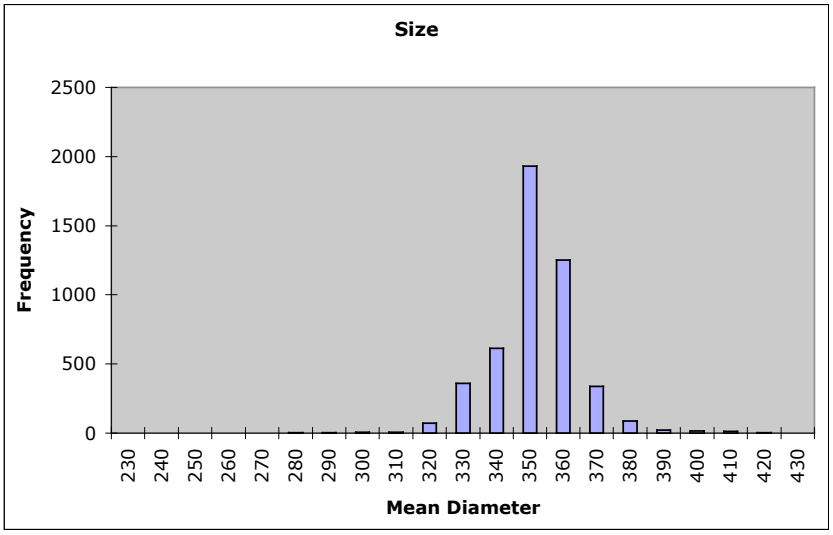

Figure 2-17: Size and shape summary for 4724 NUCO kernels measured at twice the magnification of previous measurements. Measurements are in μm from edge to edge through best circle fit center.

	Minimum Radius of Curvature	Maximum Radius of Curvature	Mean Deviation in Radius	Maximum Deviation in Radius
Average	117	222	1	20
Standard Deviation	28	37	1	3
Minimum	22	123	0	1
Maximum	173	492	8	53

Ave. Mean Radius = 173

Minimum Radius of Curvature	*Frequency*
20	0
30	59
40	81
50	51
60	70
70	104
80	158
90	217
100	329
110	398
120	506
130	821
140	1041
150	695
160	173
170	19
180	2
190	0
More	0

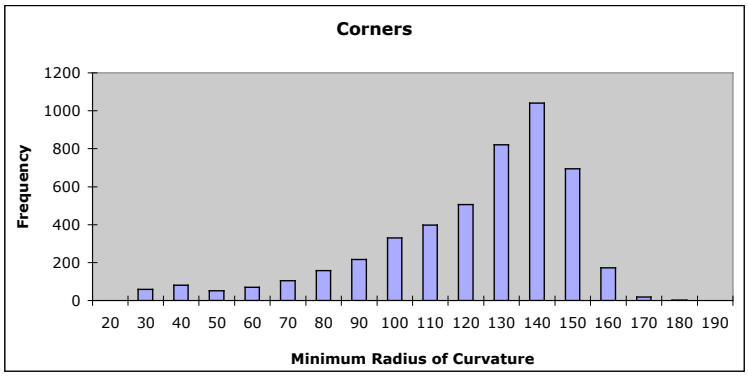

Maximum Radius of Curvature	*Frequency*
100	0
125	1
150	4
175	74
200	1241
225	1843
250	808
275	376
300	158
325	103
350	52
375	27
400	17
425	9
450	7
475	2
500	2
More	0

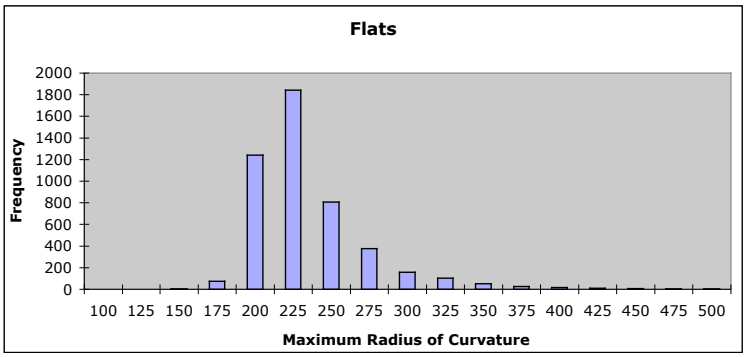

Figure 2-18: Summary of other methods of measuring the shape for a sample of kernels measured at twice the magnification of previous measurements. Radii are in μm.

There are several ways to correct for the offset error in the aspect ratio measurement. Changes in the image analysis are being considered which will apply local averaging to minimize the weighting effect of the measurement uncertainty on the uncertainty in the maximum and minimum values. It is also not unreasonable, based on the calculation above, to simply subtract out this systematic error. Figure 2-19 shows the diameter summary for the NUCO kernels with a correction of –0.006 applied to the aspect ratio. This correction was based on the expected range for the offset error ($2\Delta R/R_{mean}$) coupled with the observed minimum aspect ratio values, which were expected to be close to unity.

The histograms in Figure 2-19 were plotted with regard to the kernel product specification to show the values for the kernels that met the specification. Note that the bin values in the histograms are upper limits on each bin. The measured kernels had a average mean diameter of 347 μm with a standard deviation in the distribution of 13 μm. Based on variable sampling statistics using a two-sided student's t distribution (t=1.96), the average mean diameter of the NUCO G73B-NU-69300 composite of kernels was 346-347 μm with 95% confidence. Applying a two-sided tolerance factor test (K=2.576), the critical range containing 99% of the composite was 313-380 μm with 95% confidence. Applying a one-sided tolerance factor test (K=2.326), the critical range containing 98% of the composite (1% above and 1% below) was 317-377 μm with 95% confidence. These values were well within the specified limits of 350±20 μm on the mean and <1% below 300 and <1% above 400 μm. The composite failed to meet the specification on sphericity of <1% with $D_{max}/D_{min} \geq 1.05$. Applying a z-factor test (which is relevant for a sample size greater than 891) it was calculated that the minimum control limit that the composite would pass at <1% tolerance was $D_{max}/D_{min} \geq 1.09$. Alternately, the minimum tolerance limit for a control limit of $D_{max}/D_{min} \geq 1.05$ was 5.4%.

	Dmax/Dmin	Mean Diameter	St. Dev. In Diameter	Minimum Diameter	Maximum Diameter
Average	1.020	347	2.1	342	351
Standard Deviation	0.015	13	1.3	12	14
Minimum	0.999	252	0.5	249	255
Maximum	1.167	419	16.4	416	431

Dmax/Dmin	*Frequency*
1	2
1.005	125
1.01	936
1.015	1278
1.02	825
1.025	475
1.03	319
1.035	208
1.04	153
1.045	112
1.05	67
More	224

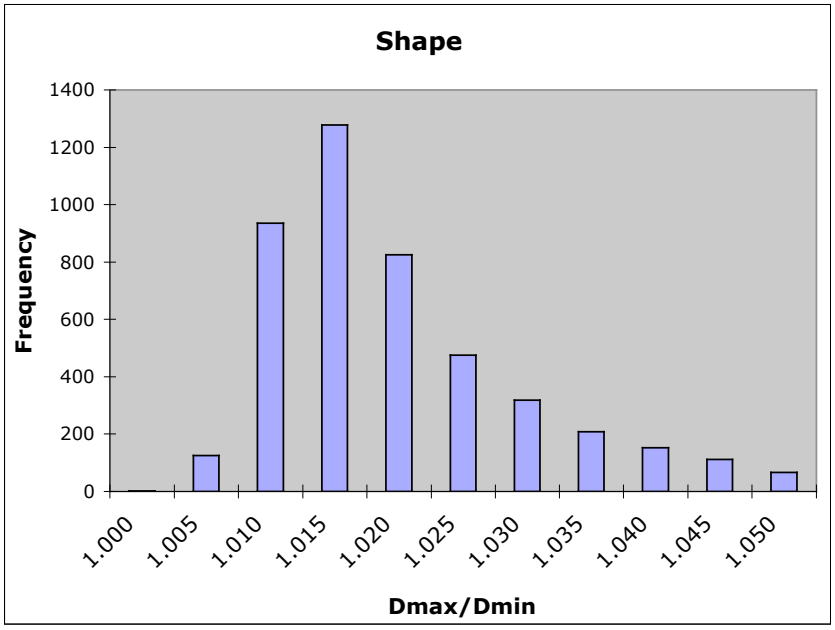

Mean Diameter	*Frequency*
300	14
305	3
310	4
315	18
320	55
325	135
330	225
335	228
340	384
345	833
350	1096
355	781
360	470
365	245
370	92
375	59
380	29
385	8
390	13
395	8
400	7
More	17

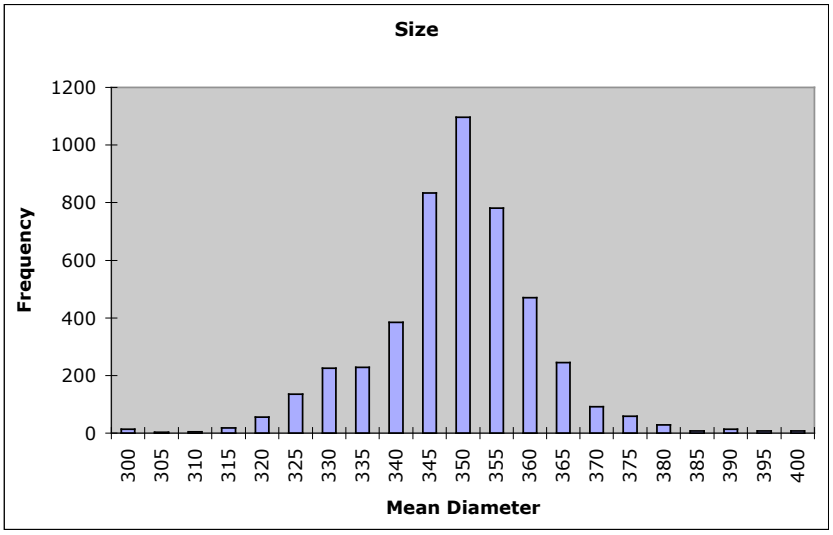

Figure 2-19: Size and shape summary for 4724 NUCO kernels. Measurements are in μm from edge to edge through best circle fit center. Plot range has been reduced to the acceptance range for the kernel specification.

2.4 Fourth analysis of 350 NUCO, repeat measurement at higher magnification using tape

Another concern with the shadowgraph method for measuring kernel size and shape is whether the kernels tend to find preferential orientation in the sample mount and how much this non-random orientation might skew the results. In order to test this effect, a sample of kernels was mounted on double-sided tape in order to prevent any realignment from the presumably random orientation in which they fell into the analysis tray. The results are shown in Figure 2-20, again a correction of–0.006 was applied to the aspect ratio. There was a shift in the average mean diameter of –0.4 μm and in the average D_{max}/D_{min} of +0.003. Given the uncertainty and standard deviations of the measurements, these deviations were insignificant considering the 95% confidence level on the sampling statistics. To a 95% confidence level, the statistical ranges for the composite calculated from the measured data for the kernels on sticky tape were as follows. The range for the average mean diameter was 346-347 μm. The critical range containing 99% of the composite was 313-380 μm. These values show no change from those in section 2.3. The composite again failed to meet the specification on sphericity of <1% with $D_{max}/D_{min} \geq 1.05$. However there were a significant number of additional kernels measured to have values above 1.05. Applying a z-factor test (which is relevant for a sample size greater than 891) it was calculated that the minimum control limit that the composite would pass at <1% tolerance based on this measurement was $D_{max}/D_{min} \geq 1.11$. Alternately, the minimum tolerance limit for a control limit of $D_{max}/D_{min} \geq 1.05$ was 7.3%. This difference, when compared to the previous measurement without tape, may be an artifact of this particular set of kernels. Because the high aspect ratios were related to broken kernels, there may be some breakdown in the assumptions of random sampling. However, it is also possible that the sticky tape method increased the likelihood of imaging very high aspect ratios on kernels which would otherwise have fallen in a more favorable orientation. The effect of using sticky tape should be studied further on particles with more typical shapes.

	Dmax/Dmin	Mean Diameter	St. Dev. In Diameter	Minimum Diameter	Maximum Diameter
Average	1.023	346.3	2.2	341	351
Standard Deviation	0.018	13	1.6	13	14
Minimum	1.001	247	0.5	239	250
Maximum	1.198	419	21.2	416	431

Dmax/Dmin	*Frequency*
1	0
1.005	44
1.01	502
1.015	1026
1.02	893
1.025	551
1.03	345
1.035	220
1.04	155
1.045	115
1.05	74
More	278

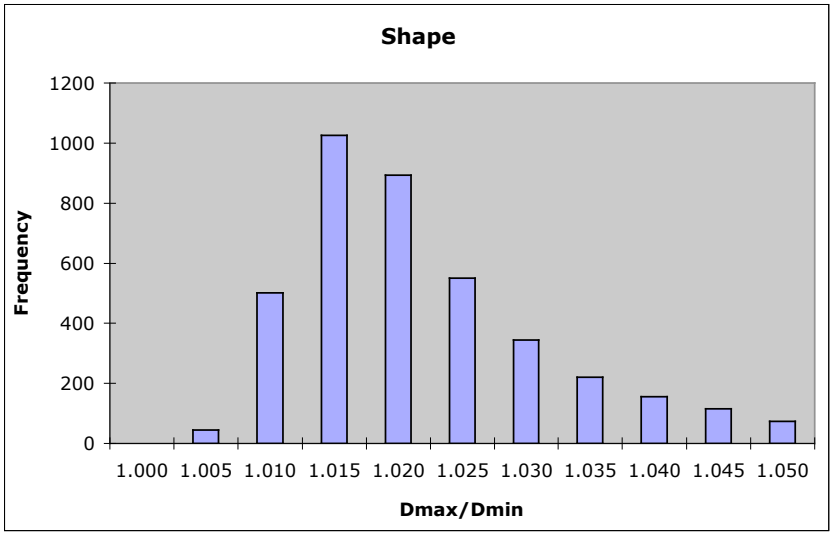

Mean Diameter	*Frequency*
300	11
305	3
310	7
315	19
320	53
325	126
330	176
335	230
340	417
345	778
350	911
355	651
360	388
365	223
370	85
375	52
380	21
385	13
390	9
395	6
400	5
More	19

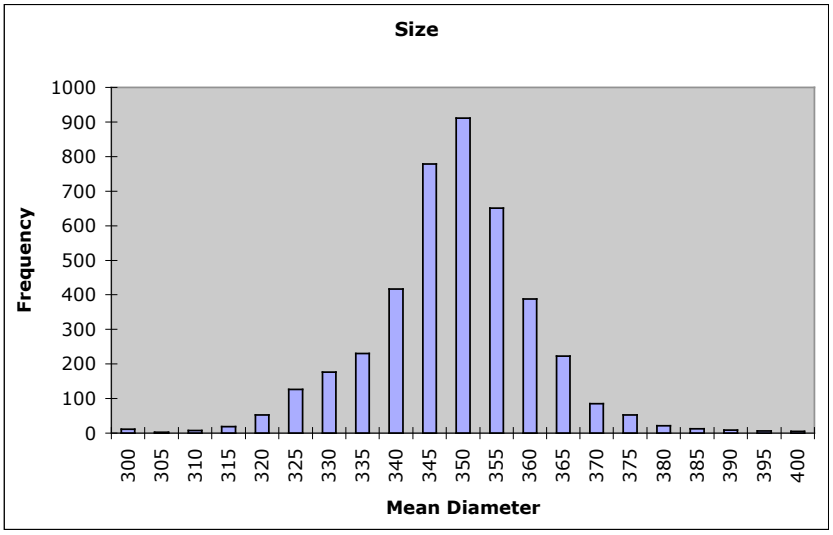

Figure 2-20: Repeat of measurement using double sticky tape. Size and shape summary for 4204 NUCO kernels. Measurements are in μm from edge to edge through best circle fit center. Plot range has been reduced to the acceptance range for the kernel specification.

3 Density Measurement

J.D. Hunn, P.J. Pappano, and D.L. Barker

Using the ASTM D3766 standard terminology, we define three different types of density: the *theoretical density* is based solely on the solid material volume, the *skeletal density* includes the closed pore volume, and the *envelope density* includes the open and closed pore volume. The theoretical density of UO_2 is 10.96 g/cc. The theoretical density of UC_2 is 11.28 g/cc. The theoretical density of UC is 13.63 g/cc.

Envelope density was measured with a Hg porosimeter. The envelope density was measured by weighing the sample and measuring the volume of mercury displaced after sufficient pressure was applied to cause the mercury to envelop each individual kernel in the sample. Open porosity information was obtained by continuing to increase the pressure and measuring the amount of mercury penetrating into the pores. Several samples were riffled from the 100 g sublot. Table 3-1 shows the results of the measurement of envelope density on these samples. The average envelope density was 10.78±0.06 g/cc with a 0.34±0.14% open porosity. Figure 3-1 and Figure 3-2 show the pore volume versus pore size measured for two samples in the table. These results are preliminary in that the uncertainty of the porosimetry measurement has not yet been fully analyzed.

Table 3-1: Envelope density by Hg porosimetry

Sample ID	Sample weight (g)	Envelope density (g/cc)	% Open pore volume
69300R-38-02-01	8.391	10.86	0.4755
69300R-38-02-02	2.807	10.72	N.D.
69300R-38-08	8.176	10.79	0.3347
69300R-38-09	8.079	10.73	0.2021
Average		10.78 ± 0.06	0.34±0.14

N.D. = not determined

Skeletal density was measured with a helium pycnometer. The skeletal density was measured by weighing the sample and measuring the volume of helium displaced by the kernel. In this technique, the helium freely enters any open porosity in the kernels. Two samples were riffled from the 100 g sublot. The skeletal density of the samples were measured to be 10.79 g/cc and 10.81 g/cc. The average skeletal density was 10.80±0.18 g/cc where the uncertainty stems mainly from the uncertainty in the calibration of the instrument. Given the 0.34% open porosity measured by the porosimeter, the measured skeletal density and envelope density are in good agreement.

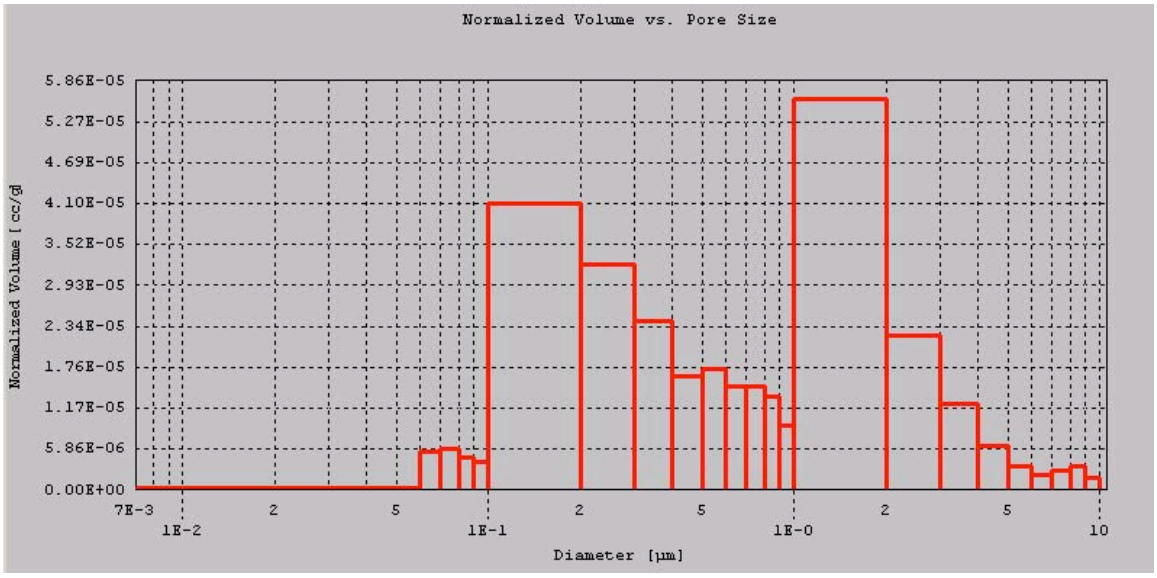

Figure 3-1: 69300R-38-08, intrusion histogram showing volume Hg versus pore size.

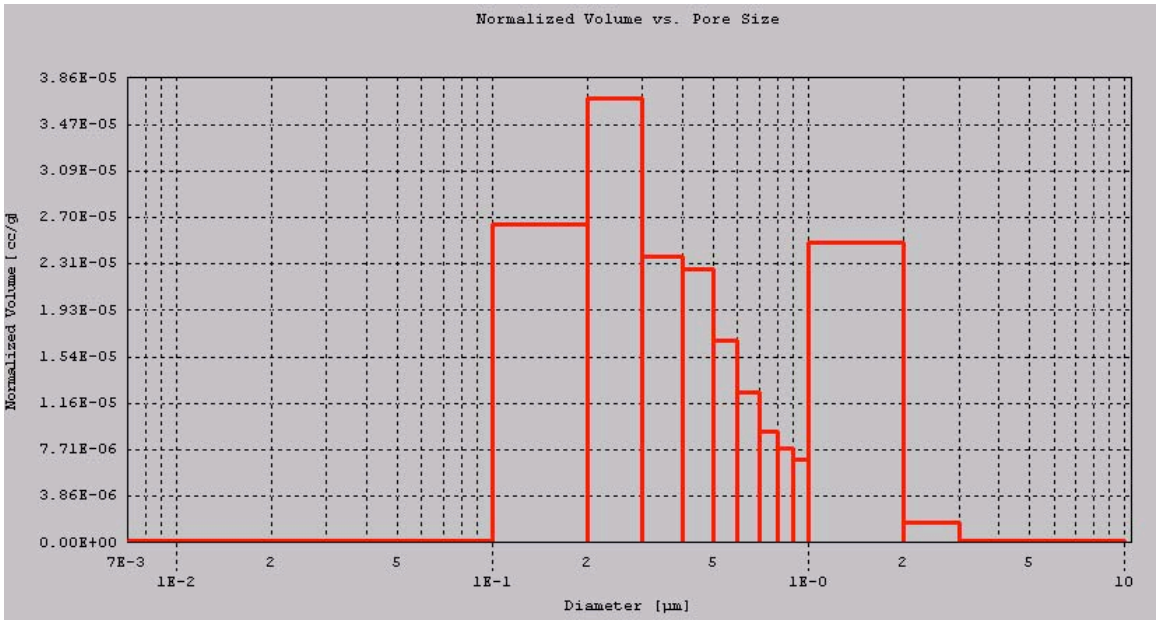

Figure 3-2: 69300R-38-09, intrusion histogram showing volume Hg versus pore size.

4 Optical and SEM Analysis of Kernel Surface

J.D. Hunn and P.A. Menchhofer

A riffled sample of NUCO kernels was observed under the optical stereo microscope (Figure 4-1 through Figure 4-3) and at least three major kernel types were evident. Type 1 kernels were smooth and shiny, the microscope's ring light was reflected as a white ring from each kernel. Type 2 kernels had a rougher, less reflective surface. Type 3 kernels were lumpy. These different kernel types probably originated from different production batches. A single kernel of each type was selected at random and the surface was imaged by Scanning Electron Microscopy (SEM). This was done for quick qualitative analysis and informational purposes and is not expected to be a statistically adequate analysis of the average microstructure of each type.

Figure 4-4 through Figure 4-6 show a kernel of the first type. The surface was very smooth and round. The grain boundaries were only partially revealed. Figure 4-7 through Figure 4-9 show a kernel of the second type. The surface of the grains was not as smooth as in the type 1 kernel. There was also a lot more relief between grains and the grain boundaries were more evident. Figure 4-10 through Figure 4-13 show a kernel of the third type. The surface was very irregular and there were some regions where the grains look smaller than those in the other types. Figure 4-14 through Figure 4-16 show what might be a fourth type of kernel. This kernel had a smooth grain surface like the type 1 kernels but had more visible individual grains like the type 2 kernels.

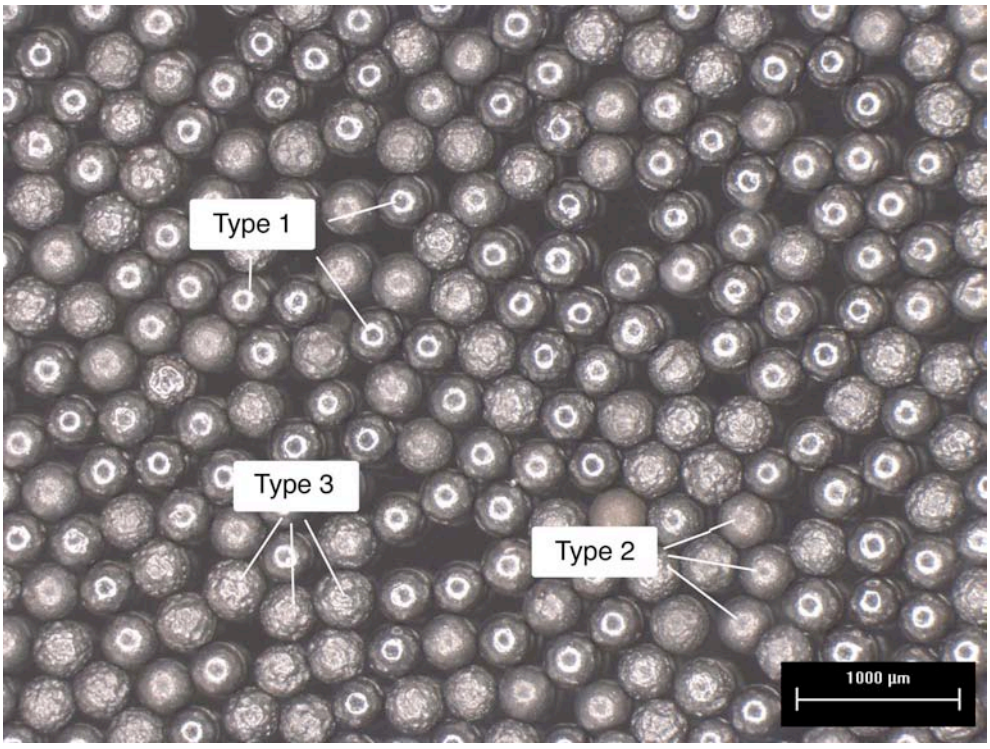

Figure 4-1: Stereoscope image of NUCO kernel composite.

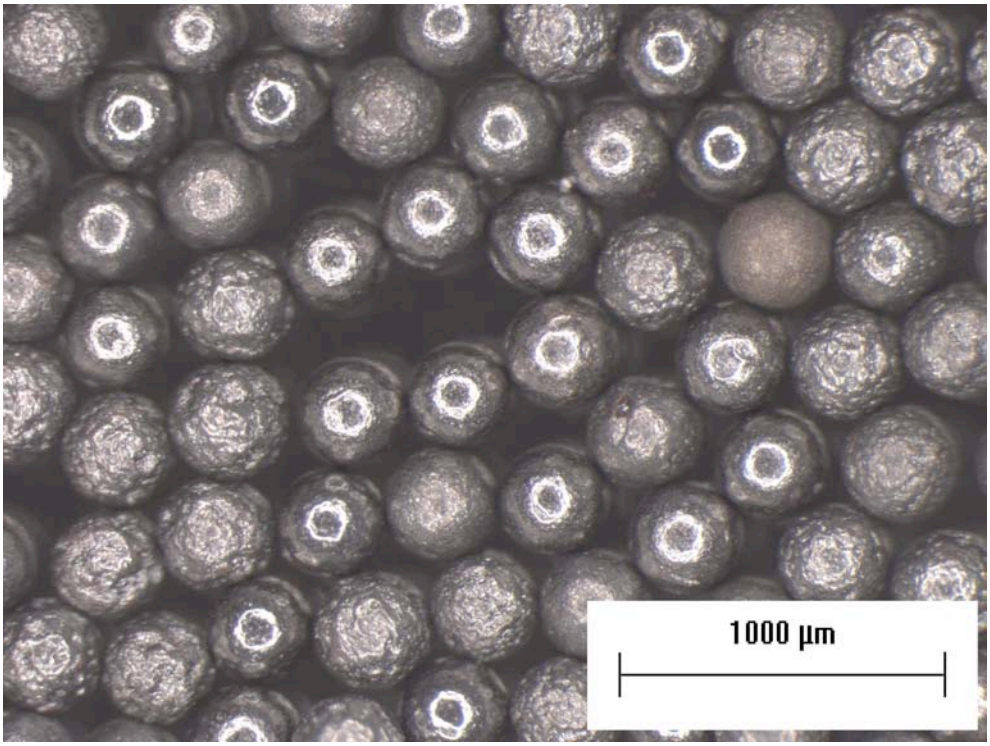

Figure 4-2: Stereoscope image of NUCO kernel composite.

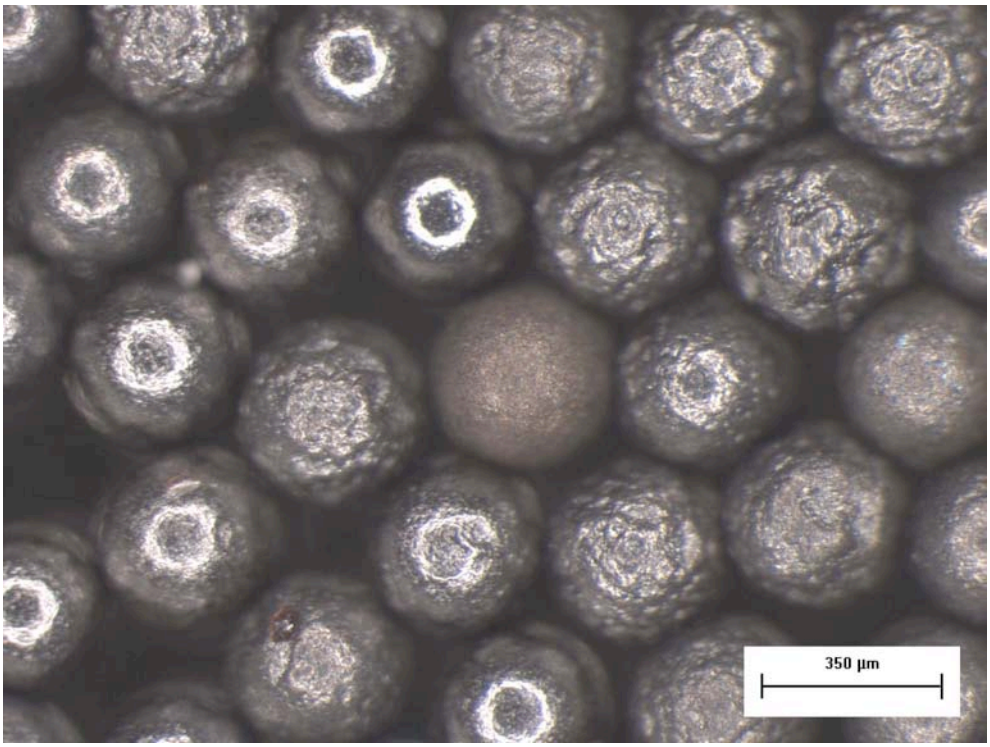

Figure 4-3: Stereoscope image of NUCO kernel composite.

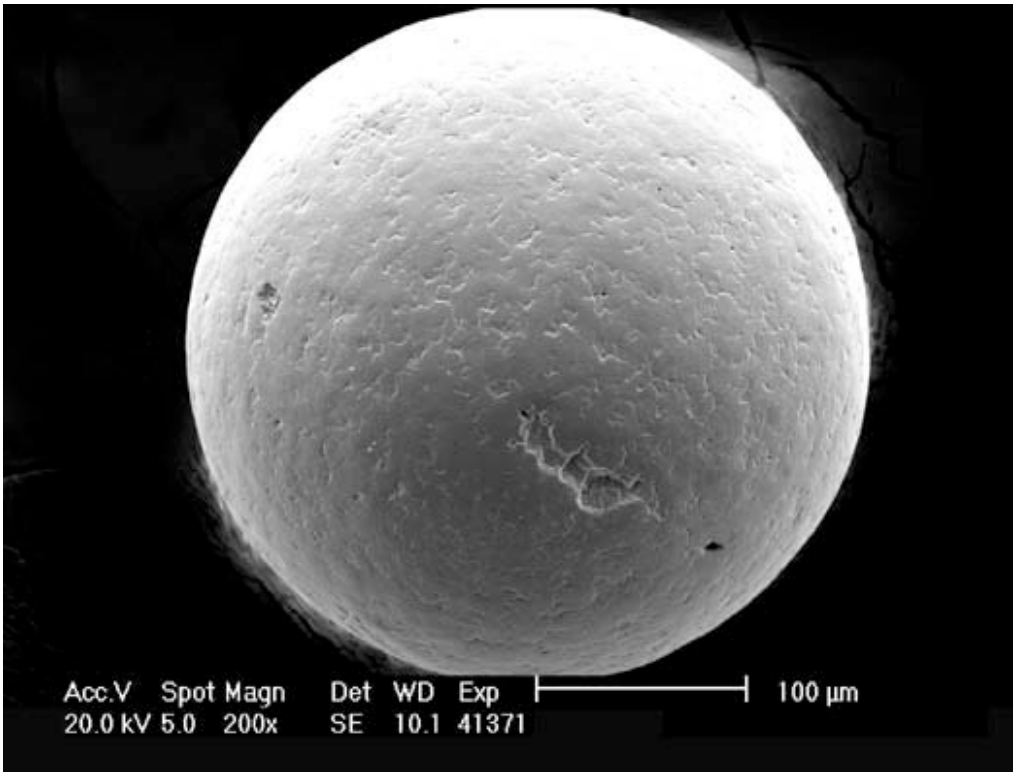

Figure 4-4: Type 1 NUCO kernel

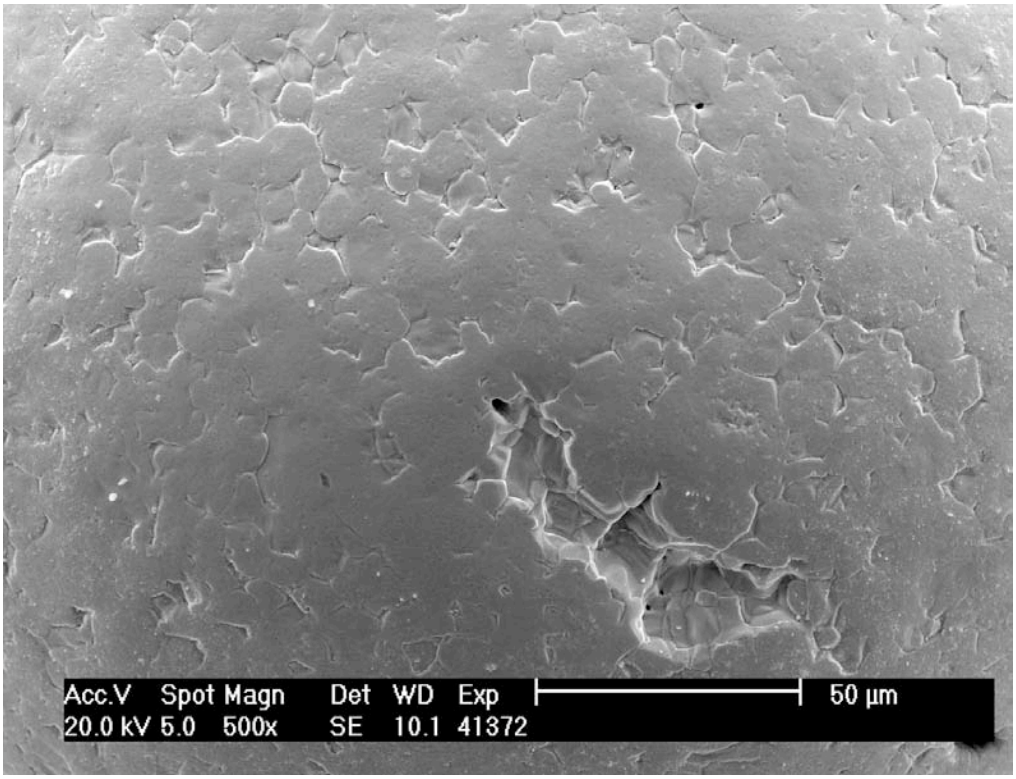

Figure 4-5: Type 1 NUCO kernel

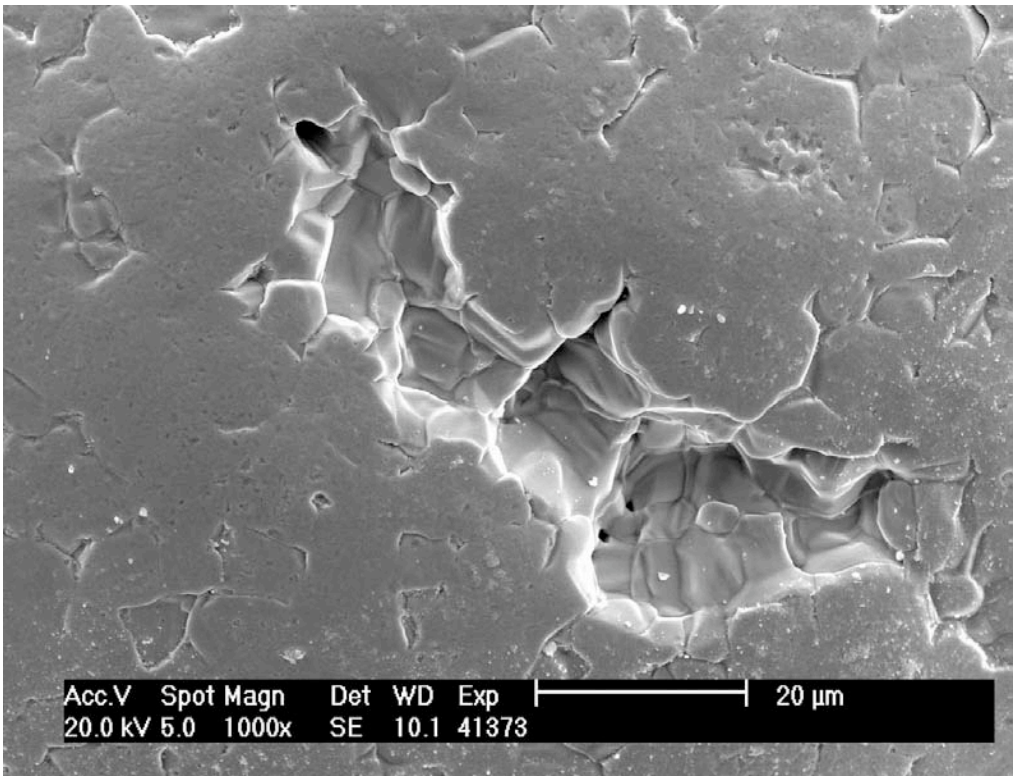

Figure 4-6: Type 1 NUCO kernel

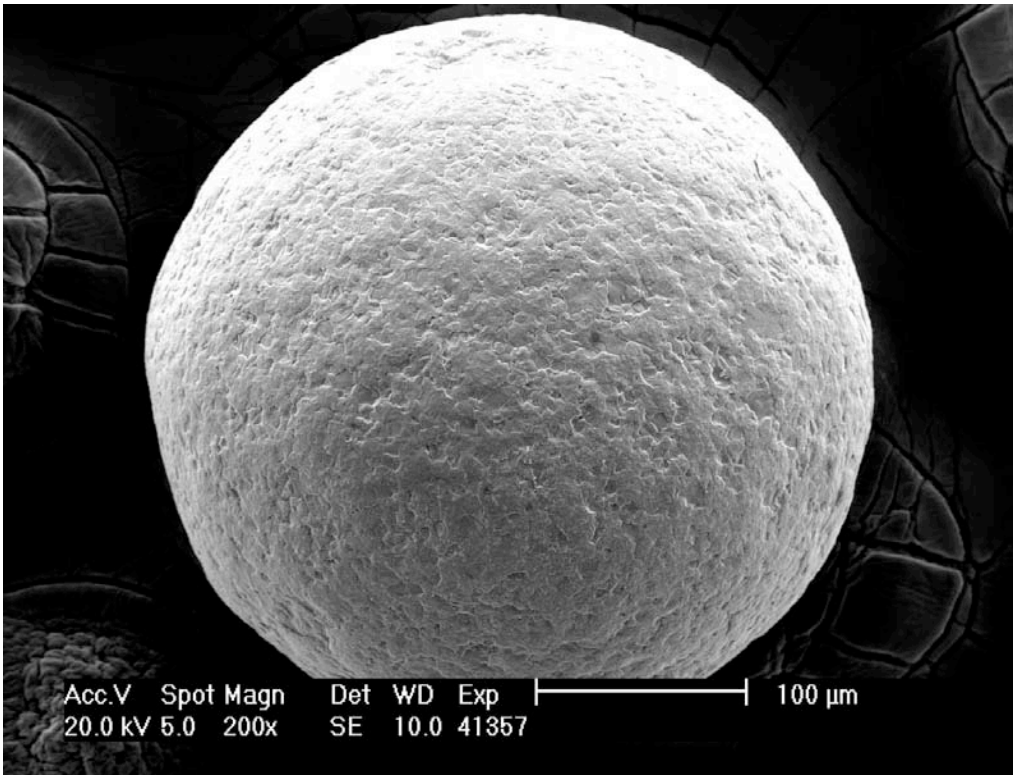

Figure 4-7: Type 2 NUCO kernel

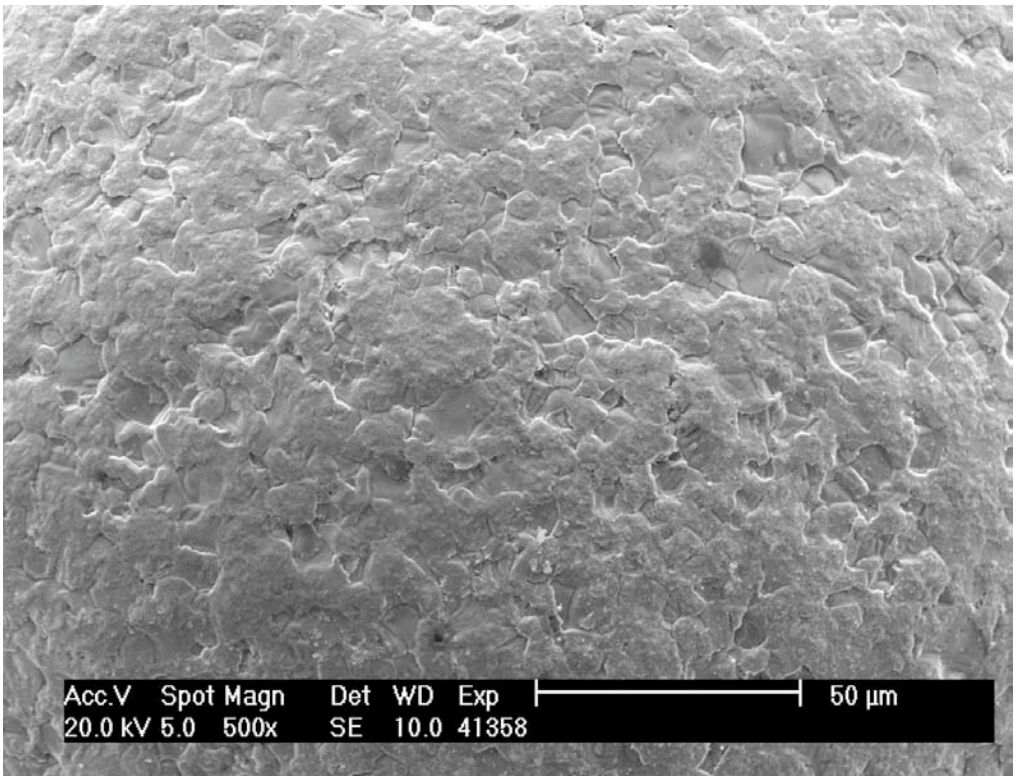

Figure 4-8: Type 2 NUCO kernel

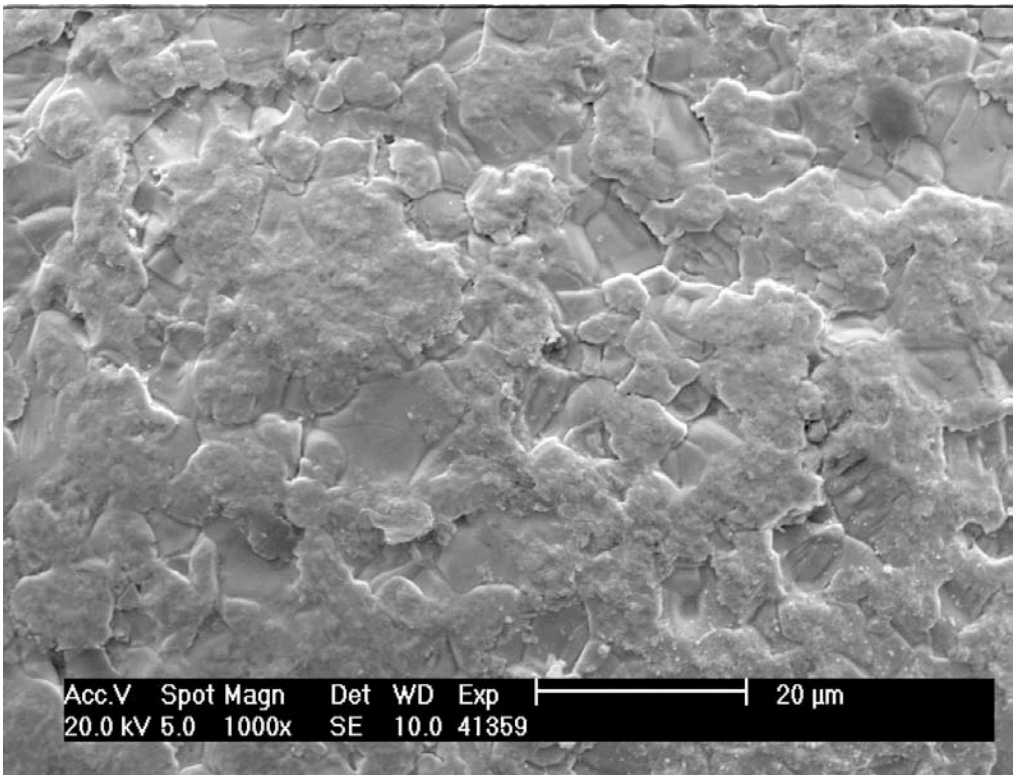

Figure 4-9: Type 2 NUCO kernel

Figure 4-10: Type 3 NUCO kernel

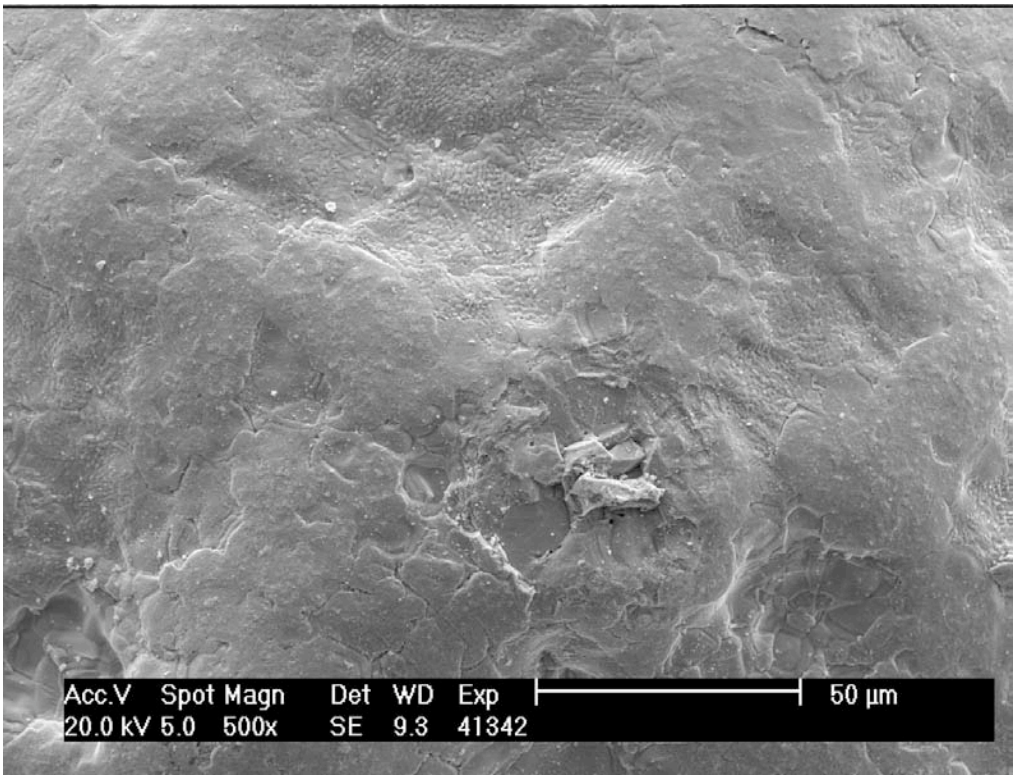

Figure 4-11: Type 3 NUCO kernel

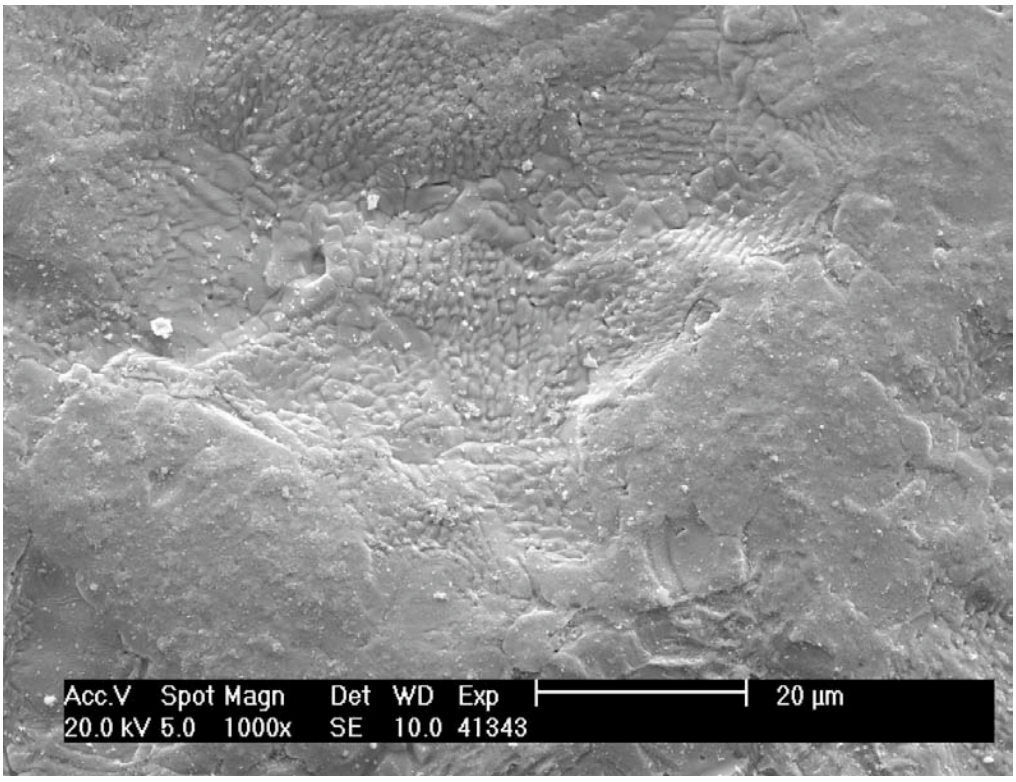

Figure 4-12: Type 3 NUCO kernel

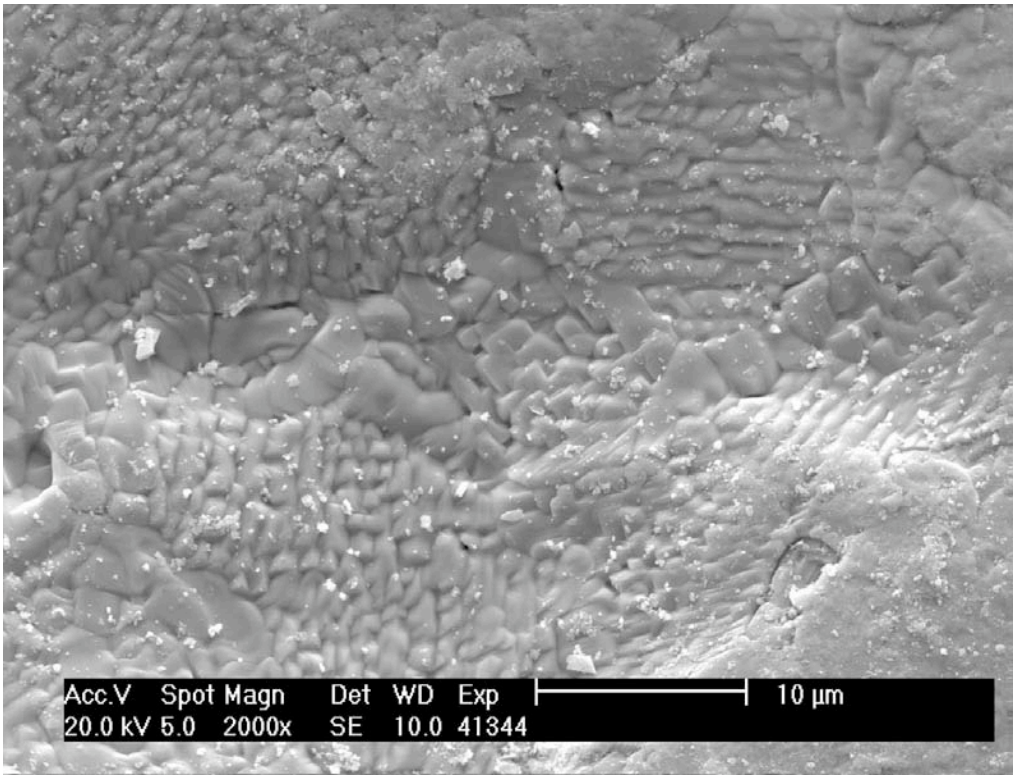

Figure 4-13: Type 3 NUCO kernel

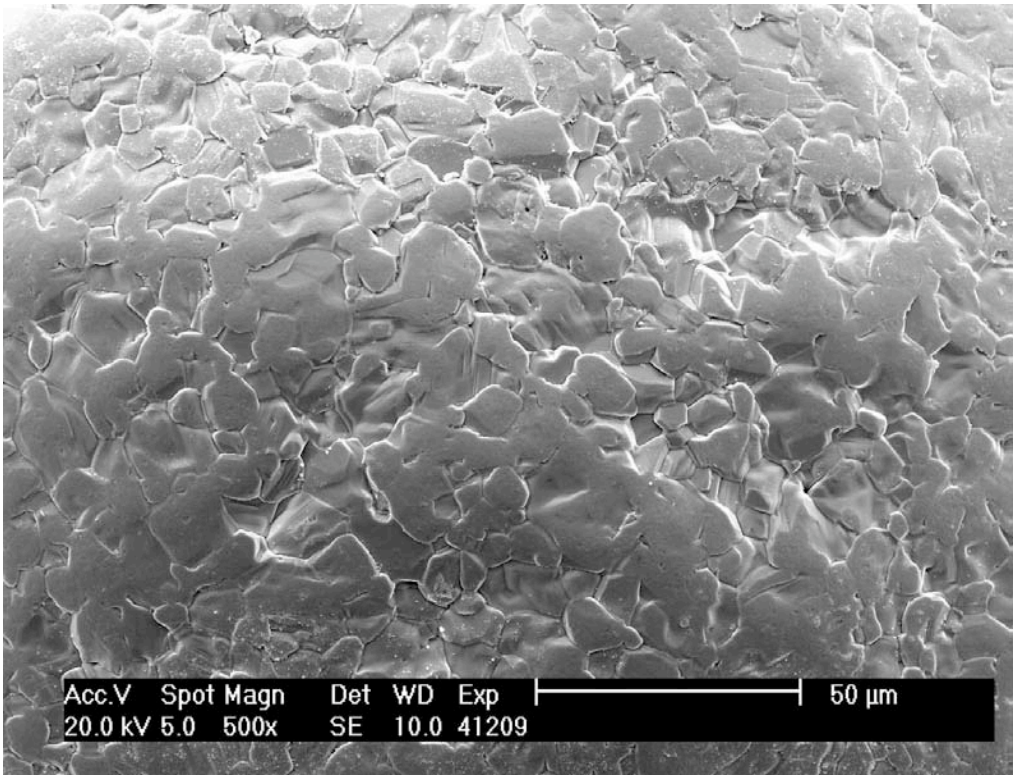

Figure 4-14: Type 4 NUCO kernel

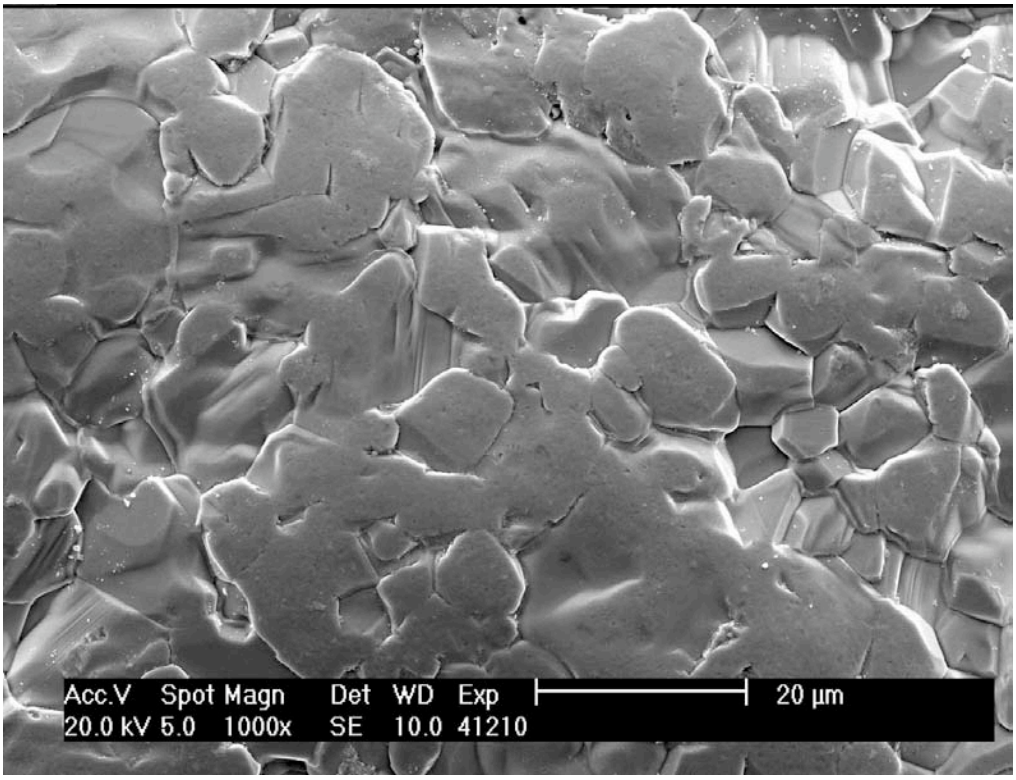

Figure 4-15: Type 4 NUCO kernel

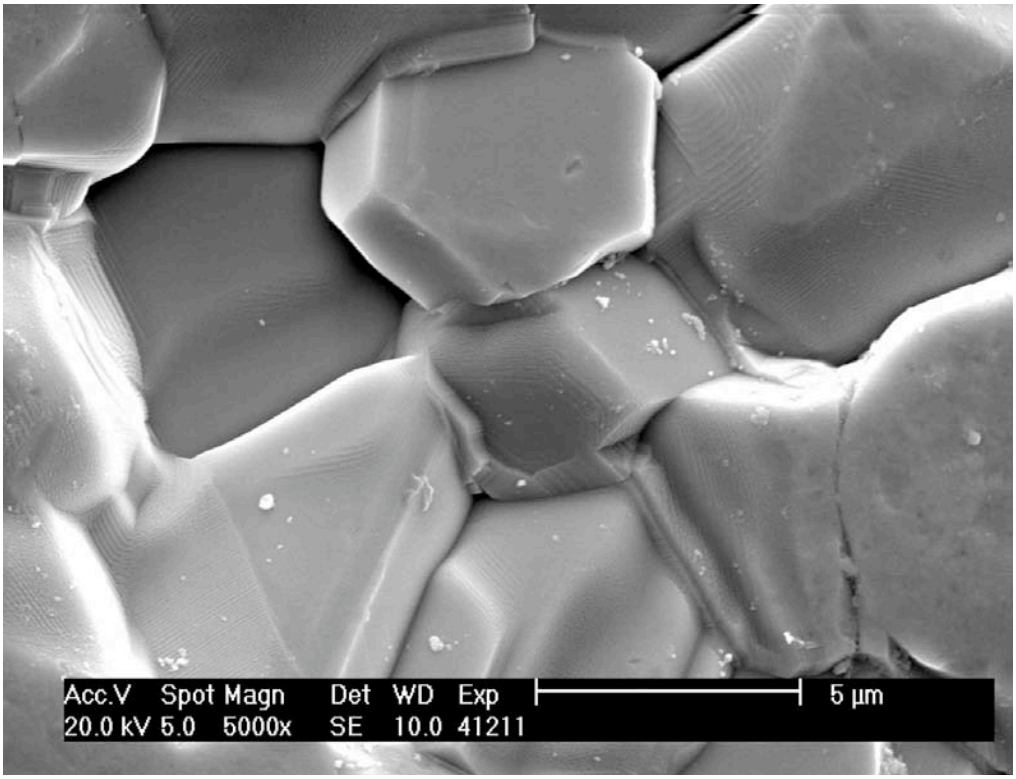

Figure 4-16: Type 4 NUCO kernel

5 Friability of Kernels

J.D. Hunn and J.L. Collins

It was observed that many of the kernels measured to have high aspect ratios were actually misshapen due to pieces that had broken off the kernel. This breakage may have occurred during handling either at BWXT or ORNL (riffling and pouring in and out of bottles) or during ground shipment between BWXT and ORNL. Several bottles were observed in the as shipped condition. These bottles all contained broken fragments. During riffling at ORNL, debris was observed and discarded if easily separated from the pourable kernels. This tended to separate out the small fragments but leave the larger, mostly whole kernels, which were subsequently imaged in the shape measurements. A bottle containing a riffled subset from 69300R-38 was shaken a few times to simulate rough handling. A significant quantity of new debris was observed in the bottle after shaking. This debris tended to be small sections which had broken from the surface. Often these chips were much greater in surface area than in thickness. Figure 5-1 shows a typical kernel where fragments have been broken off. Figure 2-12 shows an unusual case where a shell surrounding a small inner sphere was chipped off. This may be a possible source of the small kernels.

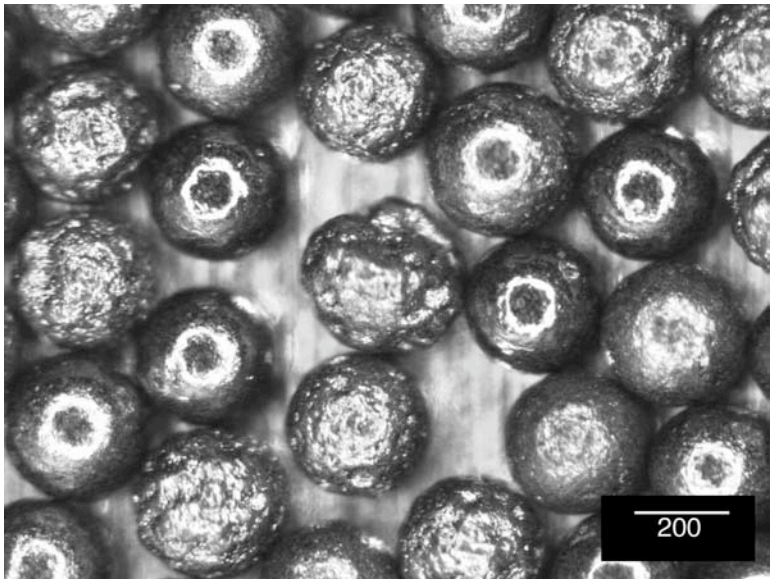

Figure 5-1: Broken kernel

A quick crush strength test was performed on 10 type 1 (smooth) kernels and 10 type 3 (bumpy) kernels. In this test, a single kernel was placed between the flats of two cylindrical rams and force applied. The maximum load for the device was 1200 g. The results are shown in Table 5-1. Although the number of kernels tested was not sufficient to give good statistics, it appeared that the type 3 kernels had a greater tendency to break. This may have been due to the fact that the bumpy surfaces on these kernels may have increased the local stress leading to fracture. In any case, the amount of failures observed below 1200 g was significant.

Table 5-1: Crush Strength of NUCO

Kernel number	Crush strength of Type 1	Crush strength of Type 3
1	>1200 g	>1200 g
2	>1200 g	810 g
3	>1200 g	>1200 g
4	>1200 g	360 g
5	250 g	>1200 g
6	>1200 g	>1200 g
7	>1200 g	450 g
8	>1200 g	>1200 g
9	>1200 g	>1200 g
10	>1200 g	>1200 g

6 Optical and SEM Analysis of Kernel Polished Cross-section

J.D. Hunn and P.A. Menchhofer

Kernels were mounted in conductive epoxy and ground and polished to near the midplane. A contrast variation across the cross section was readily observed both optically (Figure 6-1 - Figure 6-3) and by SEM using back-scattered electrons (BSE) (Figure 6-4 - Figure 6-6). This variation was due to separate oxide and carbide phases as will be discussed in the next section. The darker gray areas were oxides and the lighter areas were carbides. An oxide rind was evident on the outside surface of the kernels. This indicates a carbon depleted zone is formed during sintering. Type 1 and type 2 kernels were not readily discernible in cross section. Type 3 kernels were obvious because of their very rough surface. The oxide rind was much thicker on the type 1 or 2 (smooth) kernels (Figure 6-4) than it was on the type 3 (bumpy) kernels (Figure 6-5 and Figure 6-6). The interior of the kernels showed a mixture of oxide and carbide phases.

Pitting (black spots) were observed in the NUCO kernel cross sections. It is difficult to tell how much of the pitting is due to material removed during polishing and how much is due to porosity in the kernels. Both were expected. The friability of the kernels was very high, especially for the type 3 kernels. This made pullout during polishing very likely.

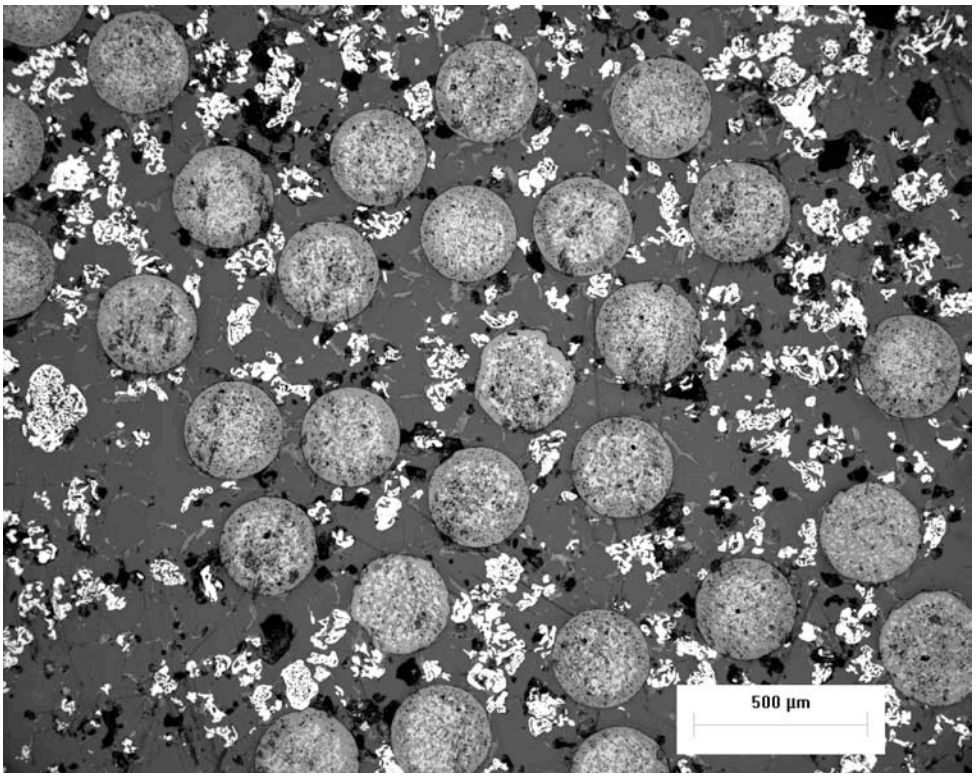

Figure 6-1: Optical image of rough polished NUCO cross sections.

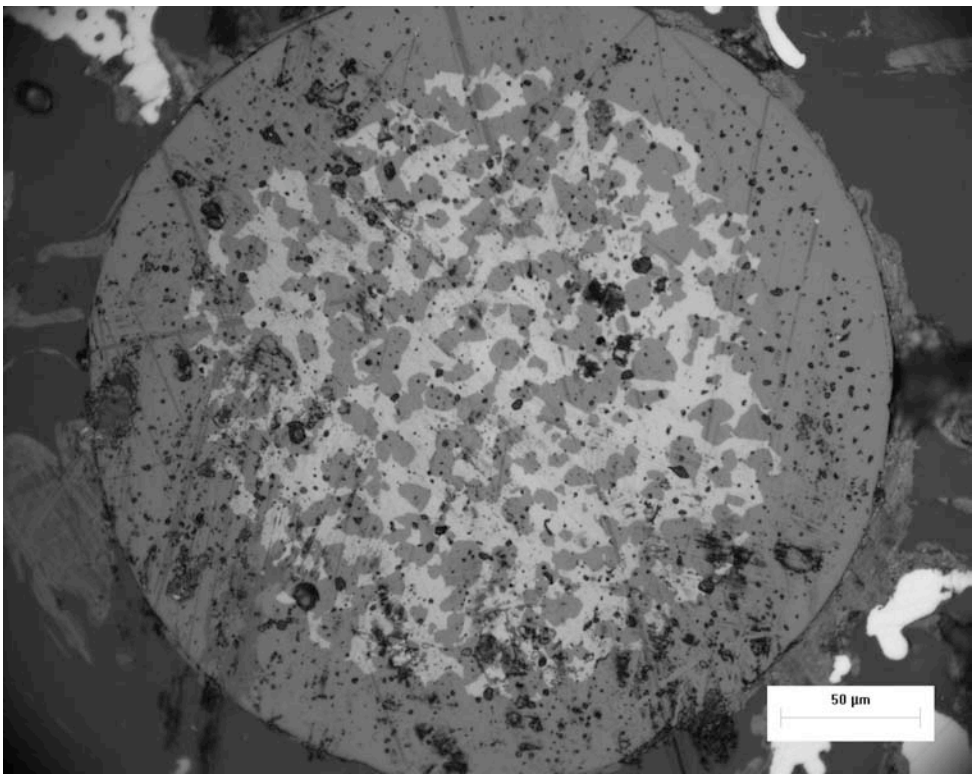

Figure 6-2: Optical image of Type 1 (smooth) NUCO kernel.

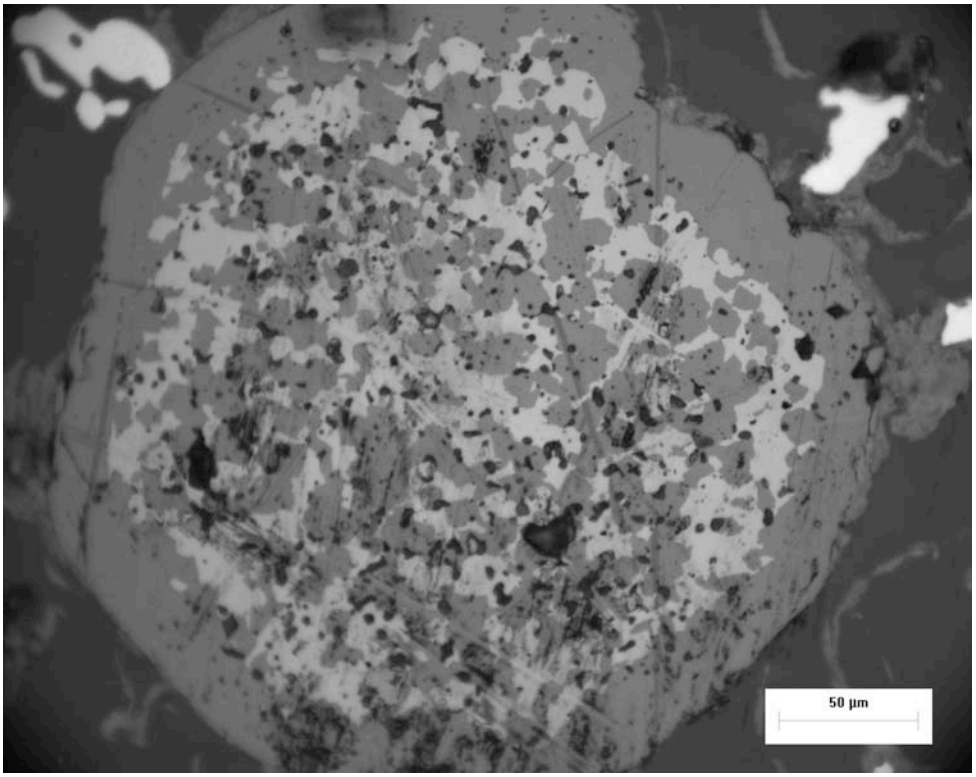

Figure 6-3: Optical image of Type 3 (bumpy) NUCO cross section.

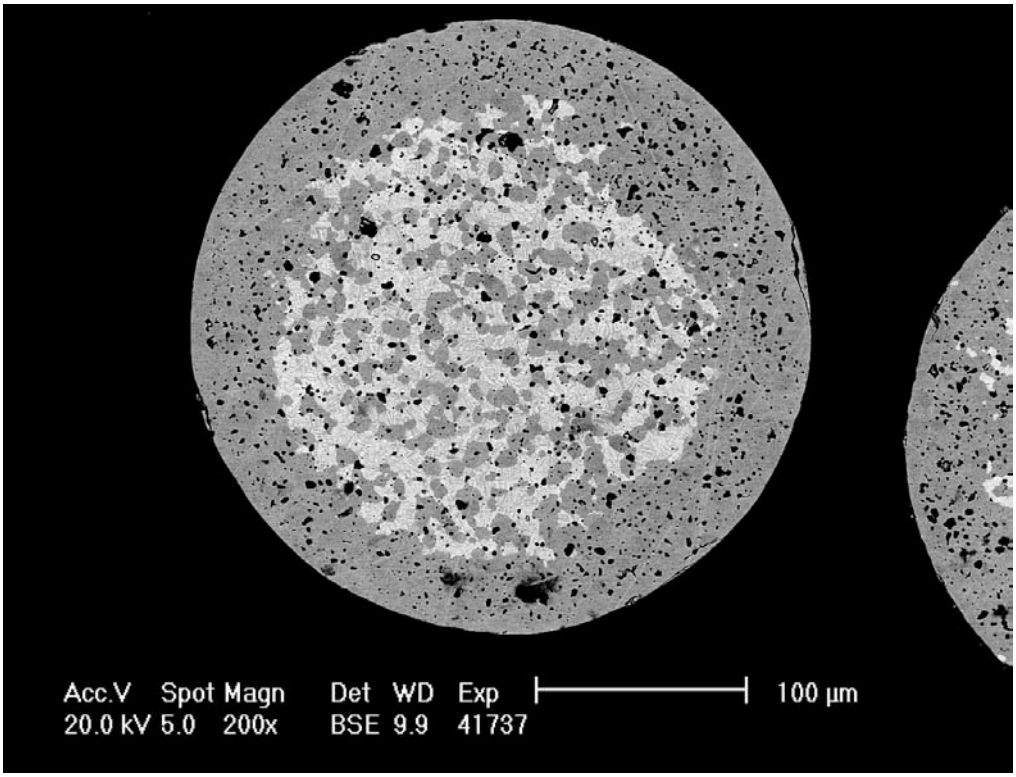

Figure 6-4: Type 1 kernel cross section.

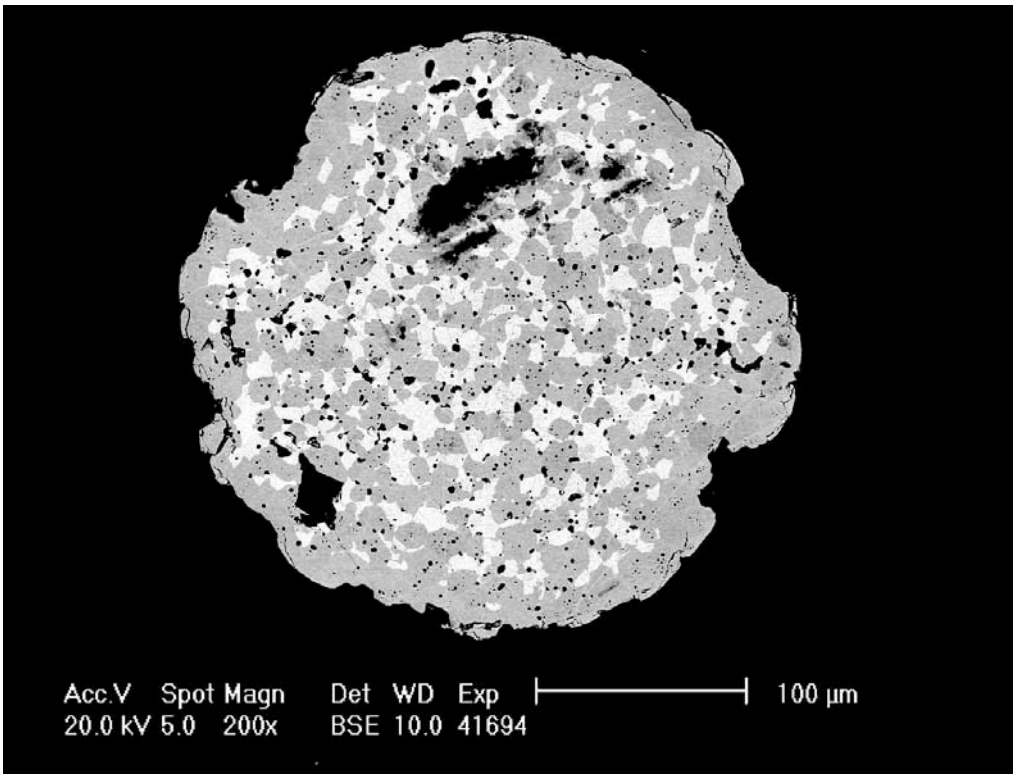

Figure 6-5: Type 3 kernel cross section.

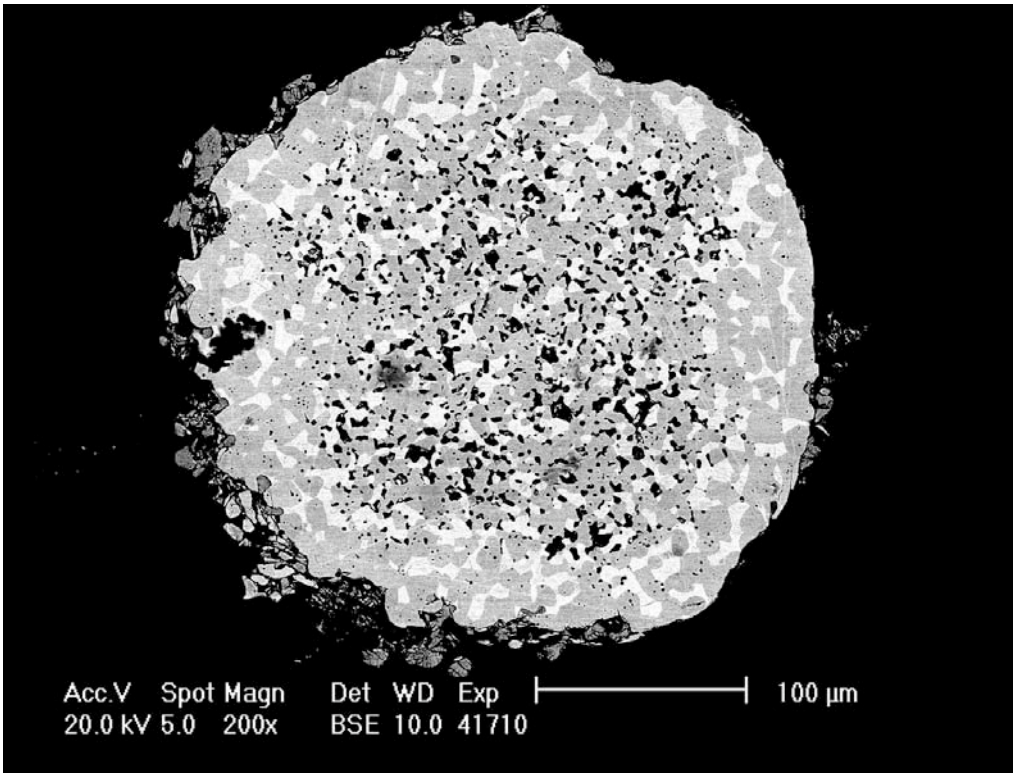

Figure 6-6: Type 3 kernel cross section.

7 EDS Mapping of NUCO Kernels

J.D. Hunn, P.A. Menchhofer, and E.A. Kenik

In order to analyze the cause of the observed contrast variation in the optical and SEM imaged cross sections, energy dispersive x-ray spectroscopy (EDS) was performed. Figure 7-1 shows a backscattered electron image of a NUCO kernel cross section. Brighter areas indicate more backscattered electrons were detected. In this case brighter areas indicate a higher concentration of uranium. The area in the white box in Figure 7-1 was scanned using EDS to produce elemental maps of uranium, carbon, and oxygen. For this technique, the sample was rastered in 0.2 μm steps over the area shown. At each point an EDS spectrum was obtained. The relative elemental concentrations at each point in the scanned area were then extracted from the thousands of spectra to form the elemental maps shown in Figure 7-2. Brighter areas in the elemental maps indicate a higher relative concentration of that particular element.

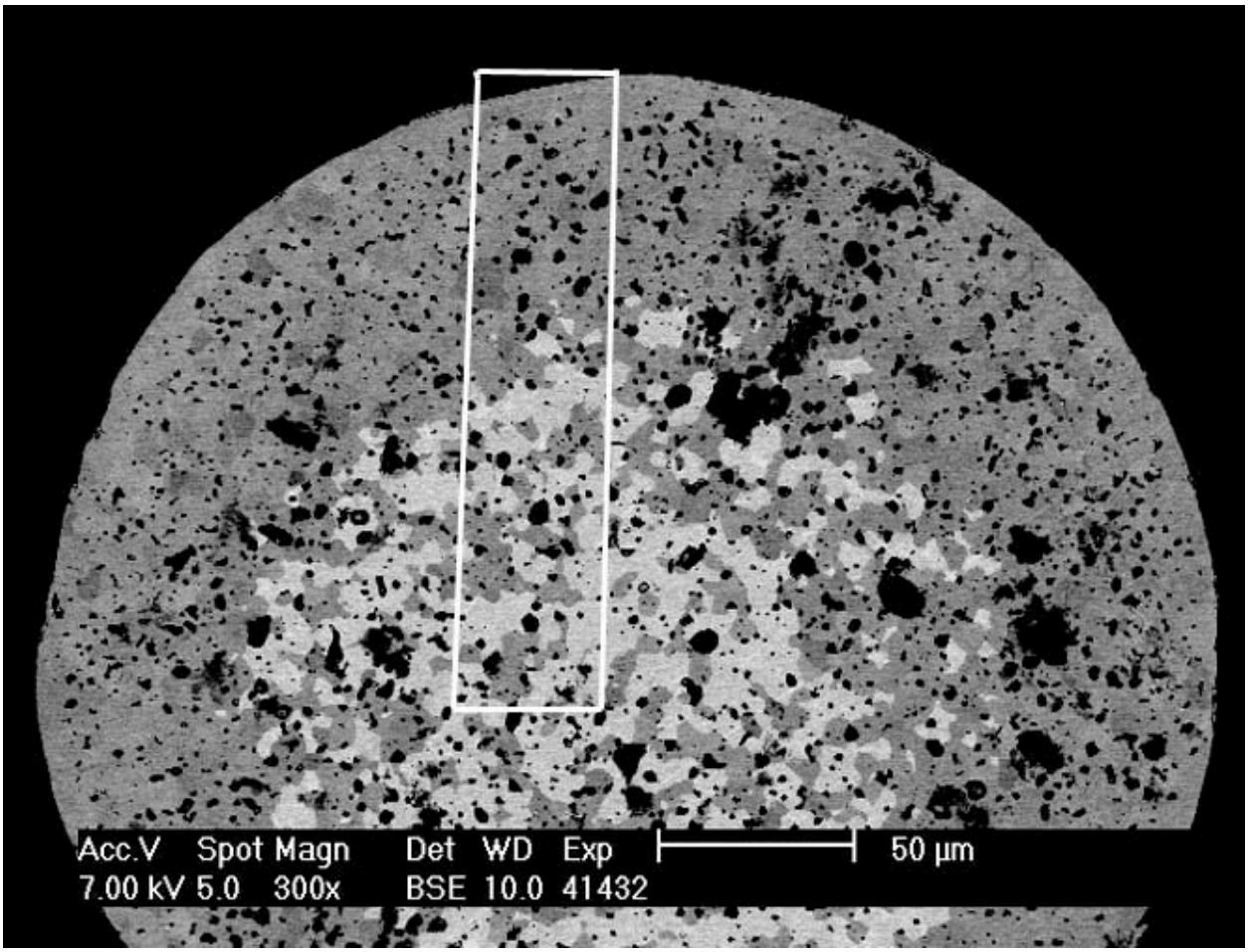

Figure 7-1: Backscattered electron image of 350 NUCO kernel cross section.

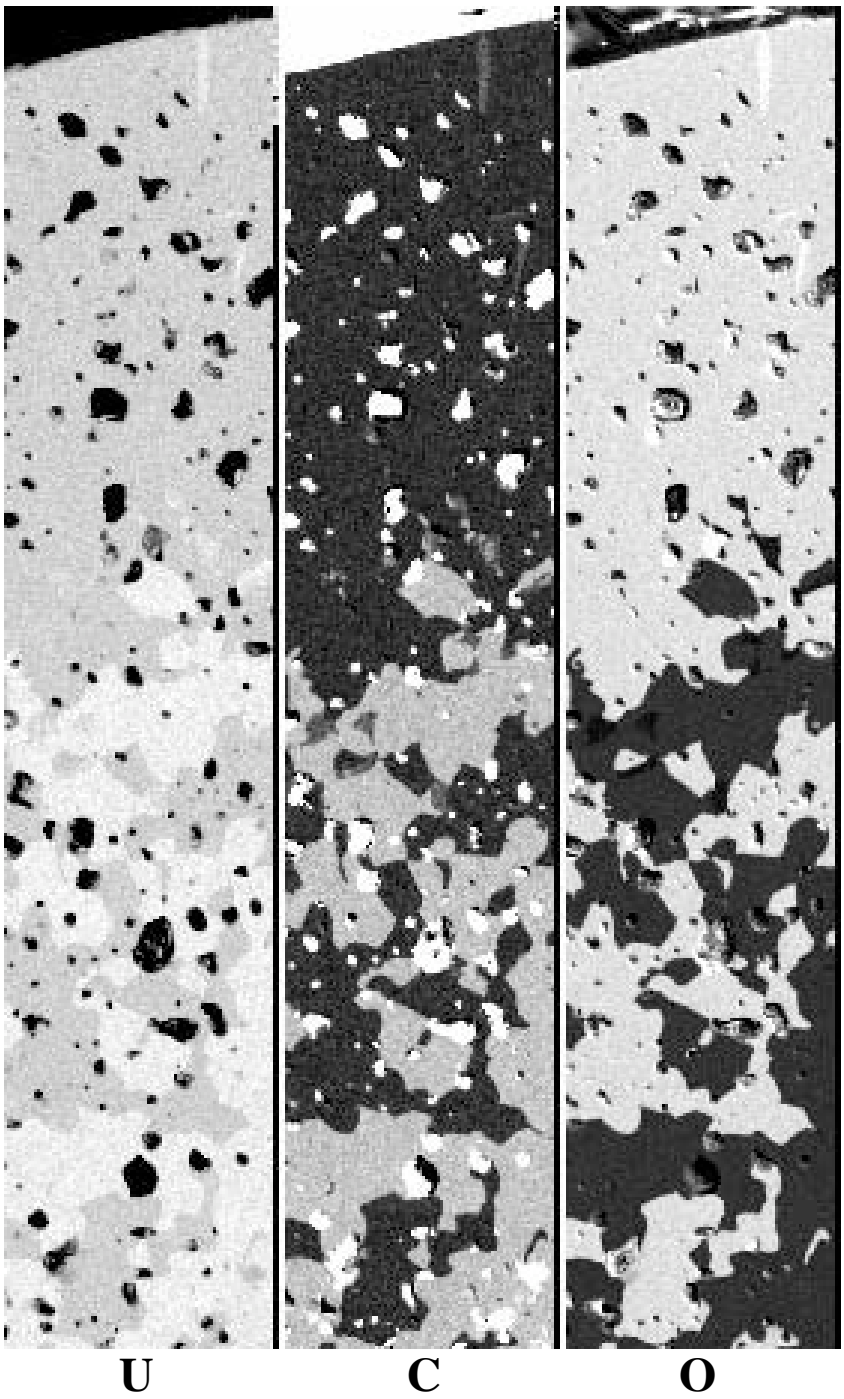

Figure 7-2: Elemental maps of NUCO produced by EDS.

The brightest spots in the center C map are probably due to epoxy trapped in surface pits since these areas do not show any uranium presence in the left U map. There is also a possibility that these areas indicate regions of free carbon, but that is less likely. In the secondary electron mode, these regions appear to be pits. The C map and the O map are inversely related. This indicates that the oxide and carbide phases are segregated. Oxide regions are dark in the C map and bright in the O map. Carbide regions are bright in the C map and dark in the O map. The carbide phases

are brighter in the U map which shows that they contain more uranium than the oxide phases. This agrees with what would be expected given the relative densities. The theoretical density of UO_2 is 10.96 g/cc. The theoretical density of UC_2 is 11.28 g/cc. The theoretical density of UC is 13.63 g/cc.

8 Oxide and Carbide Phase Composition by X-ray Diffraction Analysis

J.D. Hunn and E.D. Specht

The relative concentration of UO_2, UC_2 and UC phases was measured by x-ray diffraction. Type 1 (smooth) kernels and type 3 (bumpy) kernels were separated from the composite batch and measured separately. Measurements were made on kernels in three states: whole, broken, and powdered. Because of the limited penetration depth of the x-ray (~1 μm), these three measurements yielded different information. Measurement on the whole kernels indicated phase concentrations at the surface only. Diffraction from powdered kernels measured the average relative concentration of each phase. Measurements on broken kernels showed surface and interior phases, but with an unknown weighting of results between the two, most likely toward the surface concentration.

Samples were mounted between two pieces of Kapton tape for contamination control. The Kapton tape package was mounted on low-background Si wafers in Bragg-Brentano reflection geometry. 8 keV Cu Kα x-rays were used, with a Peltier-cooled energy-dispersive Si(Li) detector. Because the sample surface was rough, there was a dependence of intensity on Bragg angle. The whole and broken kernels only exhibited strong diffraction at high Bragg angles. The powdered kernels showed more signal over the entire spectrum but the dependence on Bragg angle had to be accounted for when calculating the relative phase concentrations. Peak areas were found by fitting the reflections to Pearson-7 lineshapes and were used for quantitative analysis by the standardless reference intensity ratio method.[1]

Whole kernels only showed diffraction peaks associated with UO_2. This was not unexpected given the results in the previous sections, where it was observed that an UO_2 rind exists on the outer surface of the kernels.

A portion of the diffraction pattern containing peaks from UO_2, UC, and UC_2 in the broken type 3 kernels is shown in Figure 8-1. Also shown are diffraction patterns calculated from the crystal structures.[2,3] Strong diffraction from UO_2 and UC are evident. The absence of either of the UC_2 peaks near $2\theta = 132.4$ implies that little UC_2 is present. The relative concentrations of the phases exposed in the broken kernels is shown in Table 8-1. These ratios are expected to still be weighted toward the UO_2 phase at the kernel surface.

[1] C. R. Hubbard, E. H. Evans and D. K. Smith, "The reference intensity ratio, I/I_c, for computer simulated powder patters," Journal of Applied Crystallography **9** (1976) 169-174.
[2] A. E. Austin, "Carbon Positions in Uranium Carbides." Acta Crystallographica **12** (1959) 169-161.
[3] R. E. Rundle, N. C. Baenziger, A. S. Wilson and R. A. MacDonald, "The structures of the carbides, nitrides, and oxides of uranium," Journal of the American Chemical Society **70** (1948) 99-105.

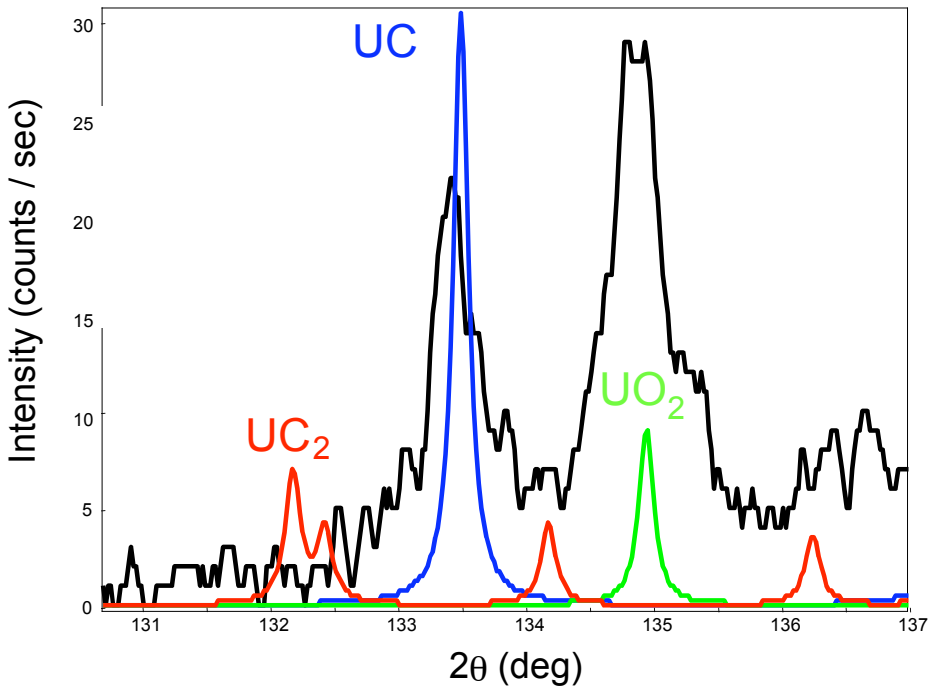

Figure 8-1: X-ray diffraction of type 3 NUCO (black) and calculated diffraction patterns for UO_2, UC, and UC_2 (color).

Kernels were ground in a mortar and pestle and the powder was distributed on Kapton tape for analysis. These results should be the most representative of the average phase concentrations in the kernels. Figure 8-2 shows the effect of Bragg angle on the measured peak intensity. The measured peak intensities were normalized by the reference intensity ratio, I/I_c, and the relative concentration of 74% UO_2 versus 23% UC calculated for a Bragg angle close to 60°. Because this plotted intensity was not constant as a function of the Bragg angle, it was important to only compare peak intensities in a limited range or to otherwise account for the angle dependent intensity when calculating the relative concentrations. This effect is presumably due to shadowing by the rough surface coupled with the short penetration depth of the x-rays in the uranium bearing materials.

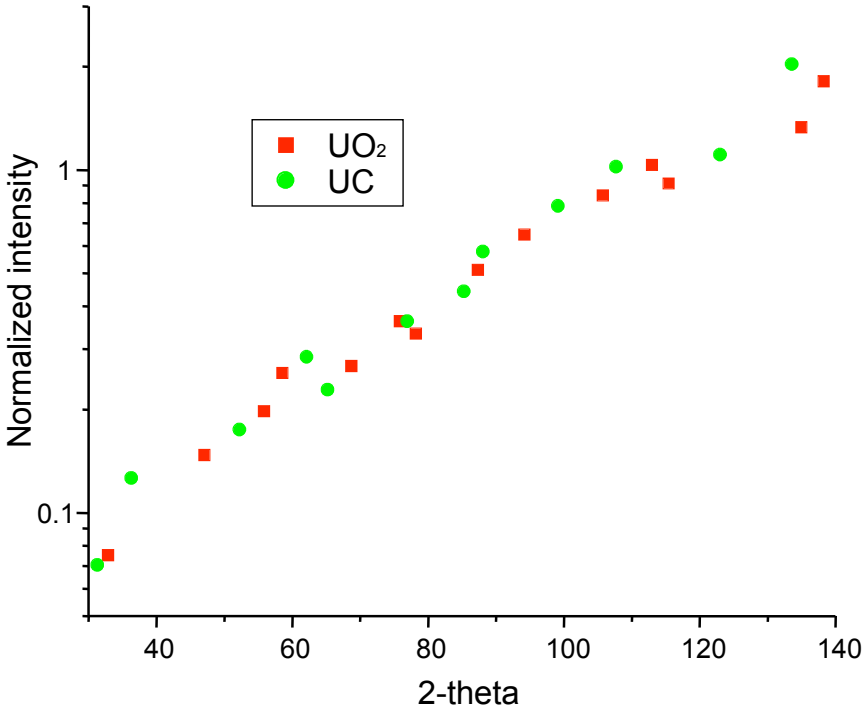

Figure 8-2: Effect of Bragg angle on peak intensity for powdered specimen.

The calculated percentages by weight of the various phases are given in Table 8-1 for the two types of powdered kernels. The dependence of peak intensity on Bragg angle was accounted for by dividing the integrated intensity of each peak by an empirical roughness correction

$$R = A + B\exp(2\theta / C),$$

where A, B and C were fit parameters. The adjusted peak intensity was then normalized by the reference intensity ratio, I/I_c, to give a value proportional to the weight fraction. I_c is the relative peak intensity calculated for each specific diffraction peak for each phase.

Table 8-1: Phase content in 350 μm NUCO (wt%). Powder results are most representative of average phase concentrations.

Phase	Type 1 - powder	Type 3 - powder	Type 1 - broken	Type 3 - broken
UO_2	69% ± 5%	74% ± 5%	90% ± 10%	84% ± 3%
UC	28% ± 5%	25% ± 5%	10% ± 3%	16% ± 1%
UC_2	3% ± 1%	1.2% ±0.4%	< 9%	< 3%

ADVANCED GAS REACTOR PROGRAM
OAK RIDGE NATIONAL LABORATORY

ORNL DOCUMENT CLEARANCE / REGISTRATION FORM

PERSON PREPARING FORM:	PHONE NO.:	DATE SUBMITTED:
Jan Z. Palmer	576-7054	June 28, 2004
DOCUMENT NO.:	**SPONSOR:**	
ORNL/CF-04/07	DOE-NE / Dr. Madeline Feltus	

TITLE:

Results from ORNL Characterization of Nominal 350 µm NUCO Kernels from the BWXT 69300 Composite

AUTHOR(s):

J. D. Hunn

SIGNATURES:

AUTHOR:

J. D. Hunn — Name: J. D. Hunn — Date: 6-28-04

TECHNICAL REVIEWER:

O. M. Stansfield — Name: O. M. Stansfield — Date: 6-25-04

APPROVER:

G. L. Bell — Name: G. L. Bell — Date: July 21, 2004